

Design, Fabrication and Test of an Apparatus to Monitor the Wetting Behaviour of High Service Temperature Brazing Materials

Rafid A. Khoja-Mendwi

A Thesis

in

The department

of

Mechanical and Industrial Engineering

Presented in partial fulfilment of the requirements
for the degree of Master of Applied Science (Mechanical Engineering) at
Concordia University
Montreal, Quebec, Canada

November 2009

©Rafid A. Khoja-Mendwi, 2009

Abstract

Design, Fabrication and Test of an Apparatus to Monitor the Wetting Behaviour of High Service Temperature Brazing Materials

Rafid A. Khoja-Mendwi

In high temperature brazing processes, the substrate wetting and the spreading of the filler metals into the joint gap is crucial for successful joining. In this work, a new approach for the assessment of the molten filler spreading behaviour is proposed based on an existing and well accepted wetting behaviour characterization method. This method is based on recording the spreading behaviour of the molten filler video-graphically, for which requires sophisticated hardware. For this reason, the remainder of the work is focused on providing the means to implement the proposed test considering the specific demands of the brazing process and the test method. Accordingly, a high temperature brazing facility with the capacity to monitor the test sample, has been designed, implemented and successfully tested to fit the purpose of the proposed test. The data collected from the preliminary tests were refined and analysed using image analysis techniques. The results of this analysis showed very promising potentials for the testing facility and the selected characterization method.

Acknowledgments

I begin my gratitude with my family for the love, wishes and support. I thank the Mandaian community in Canada for the trust and encouragements. I also express my gratitude to my friends Faris, Haider, Wadah and Alaa for sharing the hope and opportunity.

On the professional side, I start with a very special gratitude toward my laboratory and research group mates for helping me to start-up, sharing the knowledge and being my family during the study period. I thank the Mechanical and Industrial Engineering department administrative staff for their kindness and technical staff (Robert Oliver, Gilles Huard and Brad Luckhart) for their willingness, availability and friendly attitude. I thank Daniel Turner from Pratt & Whitney Canada for his sincere interactions. I also thank Dr. Philippe Bocher from École de Technologie Supérieure for his correctness. At last but not the least, I like to tell my deep regards and gratitude to my professor Dr. Mamoun Medraj for initiating the great opportunity, accepting the challenge and for the commitment.

Table of Contents

List of figures	v
Nomenclature	vii
Chapter 1 Introduction	1
Chapter 2 Background	4
2.1 Wetting and spreading of brazing filler	4
2.1.1 Non-reactive wetting and spreading	4
2.1.2 The effect of Oxygen at high temperature	11
2.1.3 Alloying element and reactive wetting	19
2.1.4 Brazing filler characteristic flow.....	25
2.1.5 Observations and motivation.....	27
2.2 An overview of the experimental techniques.....	28
Chapter 3 Apparatus.....	31
3.1 Design outline	31
3.2 The apparatus subsystems.....	34
3.3 The furnace subsystem	35
3.4 The vacuum subsystem.....	40
3.5 The argon subsystem	47
3.6 The control subsystem	51
3.7 The imaging subsystem.....	56
3.8 The sample delivery subsystem	59
Chapter 4 Testing and Measurements	61
Chapter 5 Discussion, concluding remarks, contributions and future recommendations.....	71
5.1 Discussion.....	71
5.2 Concluding remarks	78
5.3 Contributions	78
5.4 Recommendations for the future work	79
References	80
Appendix A	93

List of Figures

Figure 1 A: The viscous bending in the hydrodynamic approach B: the molecular kinetic approach [52].	10
Figure 2 The S-shape representation of the influence of oxygen on surface tension, redrawn based on Ricci and Passerone [58].	13
Figure 3 Schematic presentation of the four characteristic reaction regimes on a log-log diagram, Redrawn based on Costa et al. [64] and Ricci et al. [66].	16
Figure 4 Schematic presentation of the four reaction regimes influence on the gas-liquid metal surface exchange, Redrawn based on Costa et al. [64] and Ricci et al. [66].	16
Figure 5 The change of the characteristic velocity of the brazing filler (redrawn based on Ambrose et al. [79]).	26
Figure 6 Schematic diagram for the wetting and spreading behaviour testing apparatus.	33
Figure 7 Illustration for the furnace hot core design.	36
Figure 8 View of the furnace hot core.	37
Figure 9 View of the furnace hot core during assembly.	37
Figure 10 Illustration of the control circuit of the furnace.	39
Figure 11 External view of the furnace controller.	39
Figure 12 Internal view of the furnace controller.	40
Figure 13 Rotary vane type pump used for rough vacuum.	41
Figure 14 Oil diffusion pump used for deep vacuum.	42
Figure 15 Schematic of the layout for the vacuum and argon subsystem.	43
Figure 16 View of the vacuum subsystem tubing layout.	44
Figure 17 Standard ISO flanges used to connect between the vacuum components.	45
Figure 18 Convection enhanced Pirani gauge.	46
Figure 19 X-ray enhanced hot cathode ionization gauge (Bayard-Alpert).	47
Figure 20 View of the argon inlet line.	49
Figure 21 View of the argon exhaust and safety arrangements.	50
Figure 22 Control and communication board.	51
Figure 23 Valves and sensor synchronization board.	52
Figure 24 Control dash panel.	53
Figure 25 View of the imaging subsystem.	59
Figure 26 View of the sample delivery assembly.	60
Figure 27 View of the complete facility to monitor the spreading behaviour of the brazing filler metals at high temperature.	61
Figure 28 View of the heating panel during operation.	62
Figure 29 View of the vacuum control panel during operation.	63
Figure 30 View of the argon subsystem during operation.	64
Figure 31 View of a 1 mm sample in the furnace at room temperature.	65
Figure 32 View of a 1 mm sample in the furnace at 1100°C.	65
Figure 33 Image acquired at a lower resolution.	66
Figure 34 The steps used for image analysis.	67
Figure 35 Example of a substrate represented by a smooth line.	69
Figure 36 Example of a distorted substrate.	69
Figure 37 View of the spreading of a large drop hindered by inertia.	71

Figure 38 View of the spreading of a large drop assisted by inertia.....	72
Figure 39 The change of the height of the brazing filler drop (measured from the magnified image) with time	74
Figure 40 The change of the width of the brazing filler drop with (measured from the magnified image) time.	75
Figure 41 The change of the left contact angle with (measured from the magnified image) time.	75
Figure 42 The change of the right contact angle with (measured from the magnified image) time.	76
Figure 43 The plot of the change of the height of the drop with time on a log-log diagram.	77
Figure 44 The plot of the change of the width of the drop with time on a log-log diagram.	77
Figure 45 View of the control panel during roughing vacuum.....	95
Figure 46 View of the heating controller.....	95
Figure 47 View of the control panel during diffusion pump operation	96
Figure 48 View of the control panel during argon flow operation	96

Nomenclature

R	Drop radius
V^*	Characteristic velocity (surface tension to viscosity ratio)
Ω	Drop volume
t	Spreading time
m	Constant of
Θ_D	Dynamic contact angle
Θ_m	Microscopic contact angle
U	Wetting velocity
F_W	Contact line driving force
K°	The equilibrium frequency of the random molecular displacements occurring within the three-phase zone
λ	Average distance of each molecular displacement
γ	Surface tension
X	Mole fraction
Γ	Adsorption
ϵ°	Ratio between the metal to oxygen fluxes
Φ	Thiele modulus (the ratio of reaction to diffusion rates)

Chapter 1 Introduction

The choice of joining process for a specific application involves many different parameters such as cost, joint strength, geometry and dynamic loading. Brazing is an attractive choice when a permanent joint with high integrity is needed. It is very attractive for the applications that involve highly engineered materials that can not tolerate microstructure or shape distortion and residual stresses. Brazing provides a strong, uniform and leak proof joint and it can be the choice for joining inaccessible parts and multi component complex geometry assemblies. However, as the braze filler has a lower melting temperature than the base metal, brazing can face challenges in high temperature applications [1]. For this, nickel-based brazing alloys are well known for brazing superalloys and high-alloyed steels for high service temperature applications in industries such as nuclear and aerospace [2]. One of the main characteristics of nickel brazing fillers is it contents a relatively high concentration of metalloids (boron, phosphorus and silicon) as melting point depressants (MPD) that reduce the composition melting point to somewhere between 1000°C (1832°F) and 1250°C (2282°F) [3]. This property is put into application in transient liquid phase (TLP) bonding. This brazing technique is based on the change of the brazing seam composition through the diffusion of the melting point depressant from the brazing filler toward the base metal until isothermal solidification takes place. This technique produces joints that can perform at temperatures that exceed the brazing filler melting point [4]. On the other hand, the brazing as an industrial process can be challenged by other parameters like the process success rate and reliability. Such parameters are mostly influenced by the wetting of the work piece by the molten filler metal. As wetting is essential for the validity of the process and one of its most important

evaluation parameters, then the understanding and the ability to assess the filler wetting and spreading behaviour is essential to control the industrial process.

In its most abstract concept, the triple phase equilibrium wetting configuration was first described by Young (1805) as a mechanical balance between the energies of the involved surfaces at their common point of contact. This balance was accordingly characterised by the macroscopic angle of contact between condensed phases. At the same time, Laplace (1806) put forward the relation between pressure difference across liquid surface and its curvature. Dupré (1869) related Young's contact angle to the work of adhesion through the liquid surface tension. The three contributions set the knowledge base for the capillary flow concept [5, 6].

Brazing filler spreading and wetting of the substrate is way more complex than the simple wetting concept. Reaching the equilibrium state is arrested by solidification and spreading behaviour is usually dominated by one or more of several competing sub processes. These sub processes, permanently or temporarily, alter the real nature of the materials and their interactions at the exact interface. This is especially true in the case of brazing high service temperature alloys due to the higher affinity for diffusion, evaporation and reaction at elevated brazing temperatures. Furthermore, the influence of the trace impurities and the alloying elements can dominate the interface interactions during the process [7]. This deems the solidified or even equilibrium contact angle measurement at most non-representative and leaves the industry with no well agreed upon method to assess the wetting behaviour. For this reason, the exact relation between the process input parameters and wetting behaviour is not well established. The industrial practices are usually based on general scientific guidelines, experience and statistical

predictions [8]. In high temperature brazing, the critical areas of application and the high cost of materials imposes the need for a better characterization technique to predict the effect of the involved industrial practices during the process on its output success and reliability [9]. Accordingly, this work is motivated to propose a different way to test and evaluate the spreading of the brazing filler metal. As the new testing approach is not established yet, there is no commercially available test facility to implement such a test. This fact set the objective of this work is to provide the mean to implement the proposed test.

In this thesis, chapter 2 is dedicated to review the current understanding of the spreading phenomena and to highlight some of issues that influence high temperature wetting behaviour specifically in brazing. Based on the literature review, this study favoured one wetting behaviour characterization technique and comments on its potential importance as a testing method. The chapter ends by an overview of some of the experimental techniques used to assess high temperature spreading behaviour. Chapter 3 is focused on the design of the testing facility and the design relation to the process requirements and the components specifications. The chapter also includes details about the apparatus implementation. Chapter 4, the details of the test facility basic functions are presented and followed by the details of the results of testing some spreading samples. The method used to analyse the data collected from the real test is explained. This data is presented and discussed in chapter 5. This chapter ends with some concluding remarks contributions and future recommendations.

Chapter 2 Background

2.1 Wetting and spreading of brazing filler

2.1.1 Non-reactive wetting and spreading

2.1.1.1 Static wetting

Early attempts to shed light on the wetting and spreading in capillary joining processes were mainly focused on the relation of equilibrium thermodynamics to the success of the joining process. A good review can be found in Baily and Watkens [10] and Milner [11]. The concept of equilibrium wetting was established through the earlier studies for low energy solids and liquids, and was used to study soldering as it takes place at lower temperatures. Some of the most important issues around this concept are addressed below.

For ideal surface (smooth, homogeneous, rigid, and non volatile), Gibbs (1876) [12] suggested three conditions for equilibrium. The first is Young-Dupré equation, the second is Laplace equation and the third is the balance between the chemical potentials and gravitational intensities of the fluid components [13]. Massive contributions can be found in the scientific literature to expand the concept to include the complexities of the real surface, even though some of these efforts [14-17] ended up questioning the integrity of Gibbs and Young's approaches. Wenzel [18] proposed the addition of a roughness factor to Young equation to account for the difference between the actual surface area and the geometrical surface area (obtained from measuring the boundary that encloses the actual surface area). The factor compensate the mismatch between the net change in liquid surface area and the net corresponding change in solid liquid interface during the liquid spreading or repelling. The increase of the roughness according to Wenzel's [18]

approach has a magnifying effect on the spreading or repelling of the liquid. This treatment takes into account the effect of surface roughness with an implicit assumption that the features of the substrate surface are significantly small. Suttleworth and Bailey [19] expanded Wenzel's [18] approach and included the effect of surface features on spreading. In the course of their work, they explained the surface roughness contribution to contact angle hysteresis which is used to be attributed only to the chemical heterogeneity of the surface. Hitchcock et al. [20] studied the effect of the surface texture on a combination of high and low energy liquids and substrates under thermal and mechanical disturbance effects. In conclusion, they suggested that the increase in surface roughness will decrease the wettability of both wetting and non-wetting liquids. They suggested as well that the effect of roughening the surface reduced by increasing the liquid thermal or mechanical energy. Cassie and Baxter [21] expanded Wenzel's reasoning beyond physical heterogeneity to include chemical heterogeneity. In this treatment, the contact angle is considered to be the sum of the contact angle values for each surface domain multiplied by its fraction of the surface. Cassie [22] discussed the difference between the advancing and receding contact angle in terms of multi-molecular adsorption theory to indicate that the advancing contact angle can be unique, whilst the receding one generally less than the advancing and should not have a unique value. Li and Neumann [23] argued that in spite of the fact that Wenzel's and Cassie's treatments identified the appropriate equilibrium contact angle for heterogeneous surface, still it is not very useful. As for a heterogeneous surface there are different metastable contact angles.

To establish the relation between the equilibrium contact angle and spreading, Harkins and Feldman [24] proved that the spreading or non-spreading of a liquid can be presented through a very simple thermodynamically determined coefficient called the spreading coefficient. The spreading coefficient is the result of simple comparison of the work of adhesion between the liquid and the substrate, which drives the spreading, and the work of cohesion of the liquid which resists the spreading. According to Padday [25] the first concept of the spreading coefficient is attributed to Dupre (1869). In a tutorial fashion Youst [26] reviewed Gibbs thermodynamics of capillary, with focus on nonreactive spreading process and utilized Buff-Goodrich [27-29] vector approach to calculate various meniscus shapes and wetting forces.

2.1.1.2 Spreading and wetting dynamics

While static wetting describes the equilibrium state, the process by which the final state is achieved is described by wetting dynamics [30]. Milner [11] analyzed the brazing joint filling in analogy to the fluid flow in a pipe. The filler metal driving force was calculated from the surface tension theory and the flow resistance was determined from the fluid flow theory using Newton-Poiseuille streamline flow [31] approach. This approach is widely cited to provide some qualitative analysis to relate the measured contact angle to brazing filler spreading in spite of the fact that Milner's calculations showed that the model failed to predict even the order of magnitude of the experimental data reported in the literature [32].

Wetting dynamics as a phenomenon is a vast area of research and researchers in the field of fluid dynamics are keen on separating the different physical regimes to be addressed with key experiments and simplified analysis. For example, to reduce the gravity effect,

smaller drops can be used. The size of the system has to be very small in comparison with its characteristic capillary length in order to neglect the effect of the gravity. On the other hand, the capillary driven spreading, as an irreversible thermodynamic process, is energy dispersive. Accordingly, in most of the work done to study the capillary spreading phenomena, the driving force is calculated from unbalanced Young forces, while the energy dispersion channels is diversely considered [33]. To bring into attention the state of the art understanding of the phenomena some of the significant contributions in this regard will be reviewed. In this context Schonhorn [34] measured experimentally the rate of change of the dynamic contact angle toward its final value, for a spherical drop, and correlated it to the change in the drop radius, surface tension and viscosity. Newman [35] substituted Schonhorn's time dependent contact angle into Poiseuille's law to predict the rate of penetration in capillaries and slits. Based on these two contributions, Yin [36] derived a formulism for the spreading of a spherical cap shaped droplet on a smooth horizontal surface. He assumed that spreading is promoted by net surface tension at the interface only and retarded by the viscous friction in the bulk of the liquid. Later on Hoffman [37] tested the forced flow of silicon oils on a glass capillary where it was concluded that the apparent contact angle is a function of the capillary number. In another approach, Voinov [38] introduced formalism for the hydrodynamics of wetting. The two-dimensional motion of a liquid with a free surface was considered. In this formulism the dynamic contact angle was considered at the microscopic scale, the boundary conditions, and the scope of application for the hydrodynamic description of the fluid were established. The change of the surface energy and the work of the surface forces were considered equal to the energy dissipation due to viscosity and the energy dissipation at

the microscopic scale. Different aspects of spreading phenomena were explained based on the provided solution, including the previous findings that the spreading of liquids of the same viscosity on different smooth surfaces occurs in a similar manner. Voinov's calculations showed that for spontaneous spreading of a spherical droplet, which completely wet the substrate, the droplet radius is proportional to the time with the power of one tenth. In another development Tanner's [39] experiment revealed a relation between the edge velocity and the free surface maximum slope that occurs at an inflection point close to the moving wedge. This relation corresponds to a power exponent of $2/3$. It is concluded, based on the data analysis, that the edge velocity is approximately proportional to the cube of the slope at the inflection. In light of these contributions, Lelah and Marmur [40] tested the spreading of water and some other liquids on glass. The graphical representation of their data and some other data from the literature showed a power law relation between the spreading area and the time for both of complete and partial wetting cases. Whereas in a review of the wetting statics and dynamics, de Gennes [41] discussed the energy dissipation channels of the hydrodynamic theory and suggested that the precursor film plays an important role in the process. Based on the work of Hoffman [37], Tanner [39], and Lelah and Marmure [40], a power law relation had been proposed between time and the drop radius at constant volume and the characteristic velocity (surface tension to viscosity ratio V^*) as represented by equation (1) [41].

$$R^{3m+1} \cong V^* t \Omega^m \quad (1)$$

The contradiction between the hydrodynamic theory utilization of the traditional no-slip boundary condition, and the moving wedge led to the divergence of Navier–Stokes

equation solution were the forces exerted by the liquid on the solid become infinite. For this reason, the no-slip condition has to be released at a certain distance from the contact line [42]. Different models varied in their assumptions of the viscous dissipation mechanisms and in their treatments for the distance where the no-slip condition has to be released and in the range of contact angle treated [41, 43, 44].

On the other hand, Blake [45, 46] departed from the continuum solution in the molecular kinetic theory to utilize what is introduced as Frankel / Eyring [47, 48] view of liquid transport. Wetting is described as energy activated hopping of the molecules between adsorption sites in the three phase zone. The motion of the contact line is determined by statistical dynamics of the molecules adsorption and desorption and is assumed to be a stress modified molecular rate process. The molecules in the three phase zone have to overcome energy barriers to advance or recede, considered as the wetting line friction, while the surface tension out of balance is the driving force. The macroscopic dynamic angle is linked directly to the triple line motion. In its simplest formulation the molecular kinetic approach oversees the viscous interaction between the bulk liquid molecules. On the other hand, Voinov [38] pointed out that when the velocity is sufficiently small, the hydrodynamic effect is unimportant and referred to other phenomena to take over such as Blake's [45] liquid kinetics approach. This led other researchers [49-51] to work on hybrid models to integrate the hydrodynamics of wetting and the contact line friction together.

Blake [52] introduced a brief comparison between the different models as depicted in Figure (1).

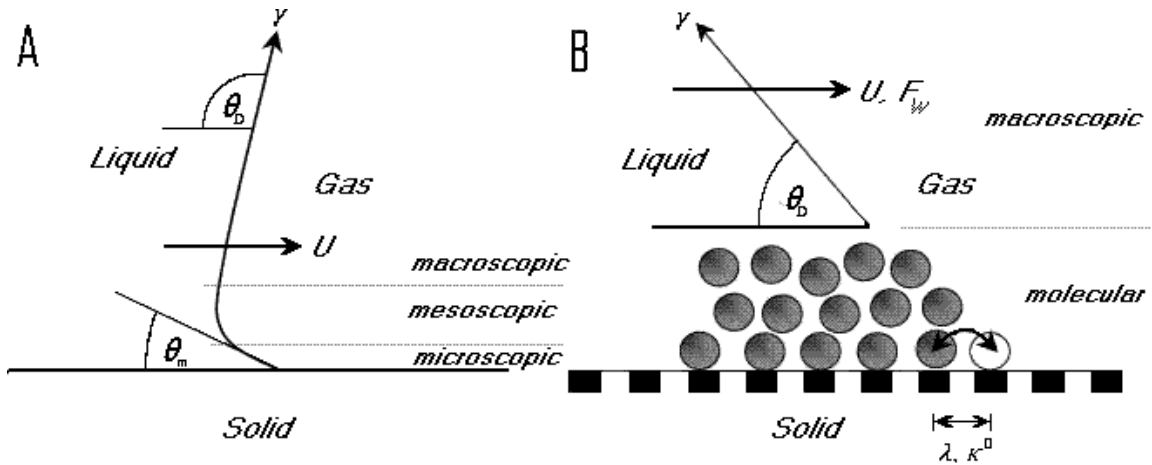


Figure 1 A: The viscous bending in the hydrodynamic approach B: the molecular kinetic approach [52].

At the beginning of the spreading process, wetting forces are still fresh and overcome easily the viscous resistance, the contact line moves fast with nearly constant configuration at the triple line. In this phase, the liquid inertia resists the motion and dominates spreading. The contact line speed is damped by the rate at which the liquid moves from the drop bulk to the triple line, driven by the difference in the capillary pressure. As spreading goes along, the driving forces decrease as well as the contact angle, accompanied by increase in the viscous friction, both leads to damp the speed of spreading and the reduction of inertia forces till the crossing to a hydrodynamic dominated wetting. Eustathopoulos et al. [53] explained based on previous experimental observations and simple calculations that for liquid metal viscous friction can be important only in very late stage of completely wetting systems.

2.1.1.3 The effect of high temperature

In an attempt to correlate between the on going efforts to understand the low-temperature spreading phenomena and the less addressed high-temperature spreading, Size et al. [54] studied the non-reactive spreading of liquid metal and oxides on molybdenum substrate,

using drop transfer technique with high-speed videography. It had been found that for liquid metals, the models based on the viscous dissipation predicted triple line speeds higher than the experimentally recorded ones. The molecular kinetic model was more representative in triple line speed prediction, temperature dependence of the liquid-solid friction, and the solid-liquid wetting activation energy. For the higher viscosity oxide droplets, the combined model used successfully to predict spreading. This led to the conclusion that the molecular interaction energies of liquid molecules, appears as a higher surface energy and work of adhesion in high-temperature liquids, play a determining role in the dominant spreading energy dissipation channel.

2.1.2 The effect of Oxygen at high temperature

In this section, some of the work done to understand the most important effects of the presence of oxygen in the atmosphere of high temperature brazing process will be discussed. It is not unusual for the researchers to emphasize on the influence of the oxygen content in the atmosphere of high temperature interfacial experiments and processes. It can be said that the oxygen content is one of the hardest to control parameters in these experiments and processes [55]. It is literally impossible to eliminate oxygen existence in the process atmosphere as it is one of the biosphere constituents and also comes out of the humidity decomposition at high temperatures. The influence of oxygen on the high temperature processes is a combination of complex effects, one or more of these effects might end up dominating the whole process. It is essential here to bear in mind that the important difference that distinguishes the surface and interfacial

properties from the bulk properties is that, a very small amount of surface active components, at the level of few parts per million can dramatically change the surface tension and its temperature dependency [56].

Thermochemistry of oxide formation and disassociation during high temperature brazing process is adequately shown in the work of Milner [11]. The equilibrium thermochemistry of oxide formation can express the energetic potential for the bulk oxidation reactions. However, a lot of work is done to establish the understanding of the kinetic and interfacial energetic influence of oxygen on the high temperature processes. Some of this work will be highlighted hereafter.

In an approach to estimate the effect of a strong surface active solute on the surface tension of liquid metals, Belton [57] represented group VI elements fractional coverage of the surface in Gibbs isotherm by Langmuir (ideal site-fillage) isotherm, to evaluate its degradation to the surface tension of liquid metals. The resulted isotherm found to be a very good representation for the available data. In another attempt using the available data also, Ricci and Passerone [58, 59] investigated the effect of oxygen on the surface tension of a group of liquid metals at constant temperature. Surface tension as a function of the oxygen partial pressure (from a very low value close to zero up to the liquid saturation) shows typical sigmoidal curves. A model was presented to describe this behaviour based on Fowler-Guggenheimer [60] isotherm and the assumptions are: 1) the system adsorption can be described by a monolayer and 2) only the nearest neighbour interactions are effective. The model considered the transfer of oxygen atoms from the liquid bulk to the surface free sites (surface segregation reaction). The dependence of the surface tension on the oxygen content is divided into three regions of the sigmoidal

curve. In the first region, at a very dilute solution, there are a large number of free sites at the surface; the surface tension shows a linear dependency on the surface composition. In the second region, when the surface oxygen concentration is sufficient enough for oxygen-oxygen atoms interactions, each atom prevents the occupation of the free sites around it by other oxygen atoms. The surface tension changes in a steep function with the surface oxygen concentration up to the oxygen maximum adsorption. In the third region, the surface tension decreases almost in a logarithmic function up to saturation where oxides start to appear on the surface of most of the metals.

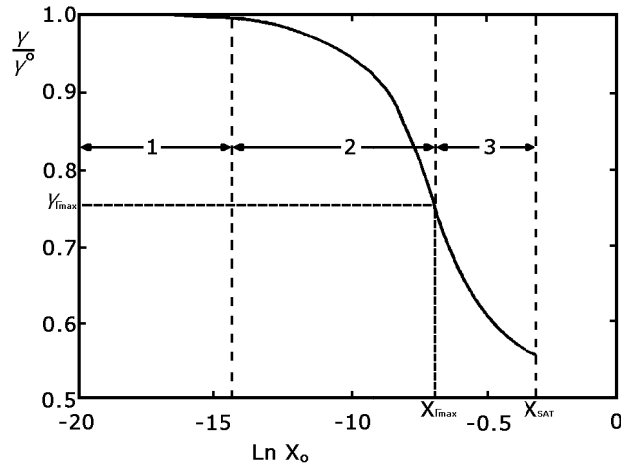


Figure 2 The S-shape representation of the influence of oxygen on surface tension, redrawn based on Ricci and Passerone [58].

Based on these contributions, Yuchu et al. [61] used Belton's [57] equation to estimate the effect of sulphur and oxygen presence on the surface tension of steels and nickel alloys. To achieve more understanding of the oxygen influence on the surface tension of alloys, Lee et al. [62] studied the surface tension of liquid Fe-Cr-O alloys at 1823K using sessile drop technique. It was found that the surface tension of the alloy decreases markedly by increasing the oxygen content and fixing the chromium content. The variation of chromium with fixing the oxygen content showed almost no effect on the

surface tension. The variation of both oxygen and chromium content showed a steeper decrease in the surface tension of the alloy with the increase of oxygen at higher chromium content. As the surface tension of Fe-Cr alloy has no composition dependence, this decrease in surface tension can be attributed to the stronger affinity of chromium to oxygen.

Surface tension degradation is not the only influence of oxygen presence in the atmosphere of high temperature metallurgical processes. Turkdogan et al. [63] concluded on a theoretical base that the rate of vaporization in a stream of neutral gas should increase with the increase of the partial pressure of a reactive gas such as oxygen. The increase of the oxygen partial pressure increases the oxygen flux towards the metal surface; this in turn decreases the thickness of the boundary diffusion layer which leads to increase the metal evaporation rate. As the oxygen partial pressure further increases, the oxygen flux toward the surface accordingly increases till a critical point where the metal evaporation rate reaches a value near the rate of evaporation in vacuum. Any further increase in the oxygen partial pressure, the flux of oxygen towards the surface becomes greater than the metal flux and surface oxides form. Experimental results verified the validity of these theoretical considerations. On a broader base Costa et al. [64] considered the rates and sequence of diffusion and reaction in the gas phase, which controls the gas-metal surface exchange, to evaluate the oxygen concentration near the surface of the liquid metal and the effective oxygen supply to the liquid phase. Based on Astarista [65], four characteristic reaction regimes were defined based on the evaluation of the Thiele modulus Φ (the ratio of reaction to diffusion rates) and ε° parameter (the ratio between the metal to oxygen fluxes). The first regime (Figures 2- and 3- a) the reaction is slow

enough not to affect the gas-metal surface exchange. The second regime (Figures 2- and 3- b) is a fast reaction with excess oxygen, in such a case all the metal vapour gets consumed and the reaction is confined near the metal surface. The excess oxygen is the actual oxygen supply to the surface. The Third regime (Figures 2- and 3- c) is a fast reaction with excess metal vapour, in this case all the oxygen is consumed and the reaction is confined to the atmosphere side of the boundary diffusion layer. The fourth regime (Figures 2- and 3- d) is instantaneous reaction and it is confined to a narrow intermediate region inside the boundary diffusion layer. Based on this approach, Ricci et al. [66] provided a kinetic-flow dynamic description for the process that might take place at the liquid vapour interface in the presence of an inert carrier flow containing definite amount of oxygen. This description leads to the determination of the possible reaction regimes based on a graphical evaluation of the relation between ε° and the Thiele modulus Φ on a log-log diagram. This approach allows the definition of the stability field for a chosen oxide. This description of the process at the interface allows a kinetic-fluid dynamic description of the system by knowing the flow parameters and the geometry of the experimental setup. The different possible regimes are illustrated in Figures (3) and (4).

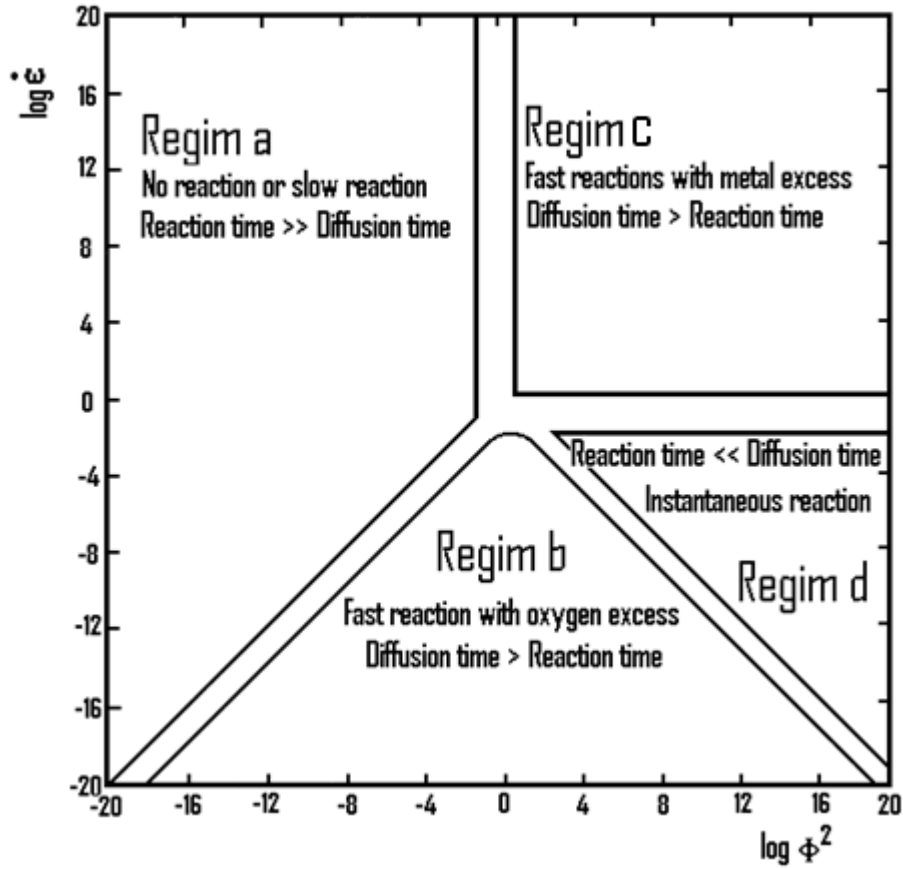


Figure 3 Schematic presentation of the four characteristic reaction regimes on a log-log diagram, Redrawn based on Costa et al. [64] and Ricci et al. [66]

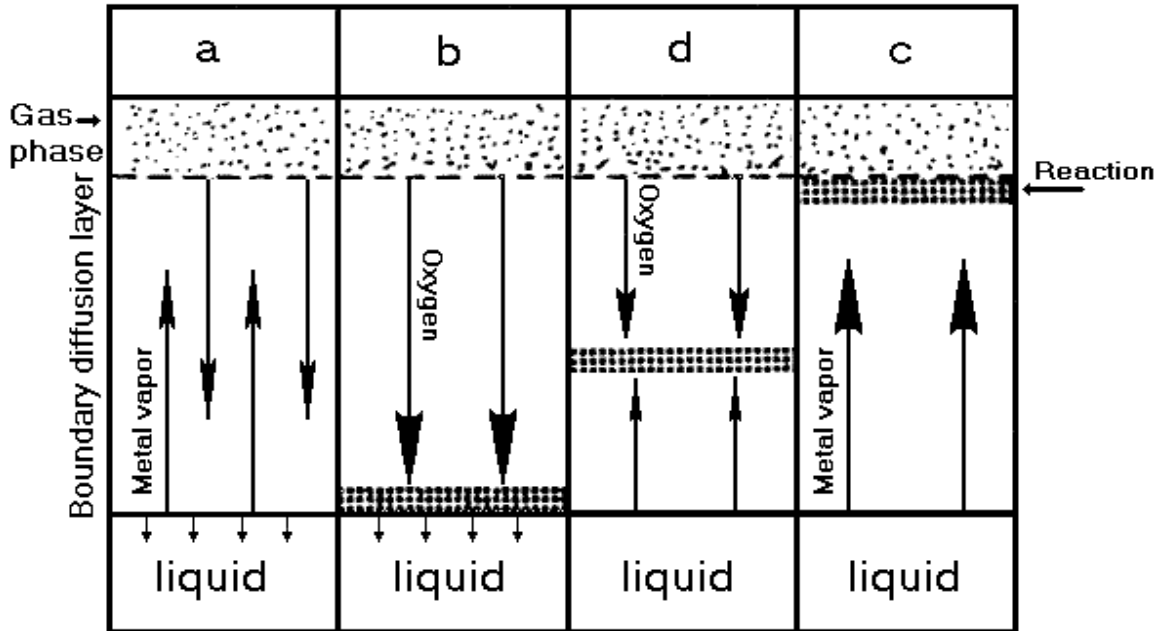


Figure 4 Schematic presentation of the four reaction regimes influence on the gas-liquid metal surface exchange, Redrawn based on Costa et al. [64] and Ricci et al. [66]

On the other hand, for a system under Knudsen regime, Castello et al. [67] modeled the process of oxygen exchange at the interface between a gas and a liquid metal. In this model, global fluxes of metal and oxygen were considered, taking into account the double contribution of molecular O₂ and the volatile oxides to the oxygen content. As the vacuum discharge keeps the system out of equilibrium, non-equilibrium steady-state conditions are obtained when the degree of saturation remains constant. Such steady-state conditions are used to express the oxygen activity in the liquid as a function of the residual oxygen pressure and the vapour pressure of the volatile oxide in the system. The thermodynamic driving force in this scenario is function of the concentration gradients. Based on each region across the interface, four steps of mass transfer were taken into account; mass transfer inside the liquid phase, liquid-interface mass transfer, interface-gas phase mass transfer, and mass transfer in the gas phase. Based on the assumption that the transport process in the gas phase has no influence on the total mass exchange at the interface (due to the large mean free path of gas molecules in a system under Knudsen regime), the interface mass transport was considered to be mainly controlled by interface phenomena and by oxygen penetration equilibrium inside the liquid. The model utilized kinetic coefficients in its thermodynamic based equations to account for the transport kinetics. The work came short in terms of justification and explanation of these coefficients.

In an effort to find the best compromise between a higher metal evaporation rate at higher vacuum and higher oxidation potential at higher atmosphere dew point, Sakamoto [68] measured the area of spreading and the final contact angle of several selected high temperature brazing filler drops and substrates as a function of the pressure and the inert

gas (argon) flow. It had been concluded that a very low level of atmosphere impurities can be maintained by the control of the argon flow rate and the furnace pressure in the pumping range of the mechanical evacuation without deteriorating the joint mechanical properties.

Meclean and Houndors [69] pointed out that at early stages of oxide formation the interface energies at the metal oxide and the oxide vapour interface may contribute significantly to stable oxides formation at oxygen potentials below those derived from bulk oxide thermodynamic data. For high temperature alloys that form in soluble non-vacuum degradable oxide layers, like alumina formers, heating in vacuum produces an imperfect oxide film at the surface. Wall and Milner [70] investigated experimentally the mechanism of surface oxide film removal by liquid metals in vacuum of some alumina forming alloys. By heating different specimens of different aluminum content in air subsequent to heating in vacuum, it had been observed that the ones contain more than 1% aluminum had developed a considerable oxidation resistance during the vacuum heat treat compared to these with less aluminum content. In other test, aluminum containing alloys showed a visible oxide film when heated in air, but subsequent heating in vacuum led to the disappearance of this film. It had been concluded that aluminum containing alloys encounter a selective oxidation process in vacuum where the lower atmosphere content of oxygen allows enough time for aluminum atoms to diffuse out of the bulk to form a transparent layer of alumina. A combination of the aluminum containing and selectively oxidized samples with non aluminum containing ones were used in spreading-drop test. Spreading under the oxide film was verified by the observation of lifting the oxide layer adjacent to the spreading front. Experimental observations led to believe that

metal penetrates the oxide film by vapour phase diffusion. On the aluminum containing samples the spreading process were related to the mutual solubility between the liquid metal and the substrate. While limited solubility led to good spreading, large solubility led to substrate erosion with limited spreading. The samples that contained no aluminum were not affected by solubility. It had been further noticed that if the furnace partial pressure exceeded “Critical Value”, specific for each alloy, the surface oxidizes substantially and the brazing cannot be accomplished satisfactorily.

2.1.3 Alloying element and reactive wetting

This section will be dedicated to review some of the work performed to understand the importance of alloying elements and surface reactions.

Wetting behavior and adhesion are strongly affected by the presence of oxides at the wetting front. Some alloying elements are usually added to the brazing paste to undermine, dissolve, or react with surface oxides, or at least, to improve wetting and adhesion over the oxide surface.

Skapiski [71] presented a simple model to relate the surface tension to the heat of vaporization. Based on the test of the model Skapiski concluded that the calculated surface tension values for liquid metals show a negative deviation from its experimental values. This deviation was blamed on the model shortage in counting for the contribution of the change in the electrons kinetic energy at the surface. However, Wassink [72] presented the same model (even more simplified by neglecting the surface tension temperature coefficient) for rough surface tension estimation. Based on this approach and Gibbs surface thermodynamics, the latter indicated a relation between the heat of alloying for random solutions and the interfacial tension. As the solubility at a specific

temperature depends on the entropy of mixing as well as the heat of mixing, Wassink went to evaluate the possibilities of their combined effect. This confirmed the experimental findings that metal with no mutual solubility should show poor wetting behavior. Even though this approximate model is not sufficient to calculate the wetting contact angle, the model and the argument behind it are used to explain the role of alloying elements in commercial brazing alloys. For the base metal filler combinations that are insoluble in each other, a limited addition of an alloying element that is soluble in both can enhance their wetting characteristics. It had been demonstrated that the basic assumptions of the model cease to hold for combinations that form intermetallics.

In an effort to describe the role of alloying element on the non-reactive wetting of iono-covalent oxide by liquid metal, Li et al. [73] estimated the trend of change of contact angle and work of adhesion with the concentration of infinitely dilute solution in the matrix of another metal. The monolayer model for the surface of regular solutions was used to describe the surface tension for a binary liquid metal in contact with an external phase. At first, to describe the surface tension of the liquid alloy, the external phase was replaced by vacuum. The liquid-oxide interface is then described using the surface tension model after adding the bond energy between the metal and the oxide atoms. For a system in which the molecular exchange energy over temperature ratio is very negative (or very positive) the model could only predict the sign and the order of the magnitude for the surface tension slope for high volume fraction of one constituent, i.e., for the extremes of the binary isotherm. For this reason, Li et al. [73] focused on the trend of change rather than the exact magnitude of the change. According to this model [73], it had been concluded that the adsorption of the solute at the liquid metal oxide interface

can be divided into the adsorption of the solute into the free liquid surface and the adhesion to the oxide. Based on the comparison between the surface tension and the work of adhesion of the solute and the matrix to the substrate, different types of isotherms for the work of adhesion and contact angle were considered. The authors demonstrated the applicability of the isotherm to the representative systems in the literature [73]. In conclusion, it had been proposed that a lower solute surface tension and a higher adhesion with the oxide in comparison with that of the matrix should result in lower contact angle and higher work of adhesion between the binary alloy and the oxide. Under these conditions, repulsive or attraction interaction (between the solute and the matrix) should accordingly lead to amplifying or attenuating this effect, respectively.

To study the wetting enhancement mechanism by a non-reactive alloying element addition to a system that encounter poor wettability, Kritsalis et al. [74] studied the effect of chromium addition to the system copper alumina. In this work, the first assumption that is chromia forms from the reaction of chromium with the dissolved oxygen or from the reduction of alumina was rejected based on the analysis of solidified drop in the bulk and at the interface (The micrograph of the interface showed no evidence of alumina dissolution). Still though, based on the experimental evidences the authors related the increase in the work of adhesion and the reduction of the contact angle to the oxygen mole fraction in the liquid. The reduction in the interfacial tension was related through Gibbs adsorption isotherm to the oxygen activity rather than its mole fraction. The authors showed by thermodynamic analysis that in the absence of chromia, the chromium in the alloy should result in a considerable decrease in the oxygen activity in the liquid. It means that the oxygen is not responsible for the increase in the work of adhesion. This

led to believe that the active species at the interface should be chromium monoxide CrO clusters, which were adsorbed strongly at the metal-oxide interface because of the iono-covalent character of CrO.

Aksay et al. [75] studied the wetting phenomena under chemical equilibrium and non equilibrium conditions. Based on Johanson's [15] treatment for Gibbs surface thermodynamics approach, wetting equilibrium was analyzed rigorously. This led to the correlation between the interfacial energies, the interfacial areas, and the contact angle configurations at the triple point. For wetting under chemical equilibrium conditions, the formation of the solid liquid interface was considered in analogy to the formation of a solution between the liquid and the vapor phase. The construction of this interface is considered as the result of the readjustment of the particles, which were originally part of the solid vapor and liquid vapor interfaces, to minimize the structural discontinuity and maintain equilibrium across the interface. Even though, the value of equilibrium surface tension has to be between the solid vapor and the liquid vapor value. If it is greater than both, then true interface does not form, while if it is less than both a transient condition, involving chemical reaction, will take place. It had been proposed that the specific free energy of the reaction at the involved interface contributes to the value of the interfacial tension. This contribution results in negative surface energy during the reaction, which promotes spreading or emulsification, unlike the equilibrium surface energy which always has a positive value in comparison to the bulk. Based on this argument, Aksay et al. [75] provided a detailed description of the spreading scenarios in the cases where the liquid or the solid is not saturated with some or all of the other phase constituents. The authors mentioned that the same reasoning applies to the cases where both of the solid

and the liquid are not saturated with each other's constituents and to the compound forming reactions.

To test Aksay et al.'s [75] argument, Espie et al. [76] designed an experiment that allowed the change of Gibbs free energy of the interfacial reaction, which means the change of the specific free energy of the reaction at the involved interface, while keeping the same interfacial chemistry. This was approached using a drop of titanium containing alloy, with fixed titanium activity, on three different oxide substrates that exhibit different reactivity with respect to the liquid alloy. The final measured contact angles on the three substrates are equal. The role of titanium in enhancing wettability was attributed to two effects. The first is the reaction of the dissolved oxygen in the liquid alloy to form surface active species that get adsorbed on the interface and reduce the interfacial tension, while the second is the formation of an intermetallic layer at the interface that shows better wetting characteristics than the original substrate. This led to the conclusion that the contribution of the specific free energy of the reaction, at the involved interface, is negligible to the wetting processes and the final wetting angle is that of the liquid on the interfacial products. However, Espie et al. [76] admitted that the free energy of the reaction could contribute to the wetting process in some other cases, when the reaction is heavily localized at the triple line.

To test the effect of reaction rate on the contact angle and the wetting kinetics, Landry et al. [77] compared the effect of changing silicon mole fraction as a reactive alloying element on the wetting behavior of copper-carbon and copper-silicon/carbide systems. They concluded that the reaction products of the first system (copper-silicon alloy on a carbon substrate) is silicon carbide, in spite of the difficulty to demonstrate that through

experimental analysis as it is not easy to screen carbon owing to the thinness of the reaction products layer. Based on the same experimental analysis, they mentioned that the layer of reaction products is grown outside the area of contact between the liquid alloy and silicon carbide substrate before cooling. For the second system (copper-silicon alloy on silicon carbide substrate), the analysis showed no trace of reaction except a very slight dissolution of the substrate, just enough to saturate the liquid drop with carbon. It was observed from the plot of the contact angle variation with time at the tested compositions for both systems that the final contact angle for all the studied cases is around the same value. This final contact angle was considered to be the equilibrium contact angle for the system copper-silicon alloy on a silicon carbide substrate. However, the rate of the decrease in the contact angle, from its initial value, increases with the increase of the silicon mole fraction. It had been observed for the second system that the contact angle decreasing rate is of several orders of magnitude higher than the characteristic rate of non-reactive systems, in spite of the absence of experimental evidence for reaction existence. This contradiction was justified by the existence of an oxide reduction reaction. The silicon oxide SiO_2 forms on the drop and substrate surfaces during heating, was reduced by the excess silicon in the drop to a gaseous silicon monoxide SiO which gets dissipated in the atmosphere. The comparison of the graphs reported in [77] at a 25 at. % silicon showed three distinguishable spreading stages for the first system and only two stages for the second. The first stage was considered related to oxide reduction reactions in both systems, and not a characteristic of the studied system. While the last spreading stage in both of the systems was considered for spreading over silicon carbide till equilibrium. The middle stage in the first system was attributed to the interfacial

reaction between the alloy and the carbon substrate. As the work of adhesion and the final contact angle did not change by the change of the reaction rate, it had been concluded that interfacial free energy contribution to the reactive wetting driving force is negligible. The authors proposed that the final contact angle and reaction kinetics are independent of the type of interfacial reaction that might exist beyond 100 seconds. Nevertheless, for faster reactions, the contribution of the interfacial reaction free energy cannot be excluded from wetting driving force.

2.1.4 Brazing filler characteristic flow

Ambrose et al. [78] experimentally examined the wetting behavior of eutectic Ni-P brazing filler alloy on several laboratory produced Fe-Cr and Fe-Cr-Ni work pieces as well as commercial martensitic, austenitic steels and nickel based super alloys. The spreading tests were followed by a careful examination of the sample features to predict the chemistry behind the observed spreading behavior. The resulted observations were summarized by Ambrose et al. [79] and the data were analyzed in consideration of the fundamental models of liquid flow. The log-log plot of the drop radius variations with time showed some characteristic curvature indicating sophisticated behaviors, still though the data could be fitted around a straight line with a slope of (0.13 to 0.16). For Yin's [36] model to be satisfied the slope should be 0.2 and for de Gennes [41] model to hold, the slope should be 0.1 (provided that the integration constant was neglected and the power of the apparent contact angle from Hoffman relation (m) was fixed to 3 according to de Gennes [41]). Ambrose et al. [79] tested the applicability of de Gennes' relation by presenting the data on a log-log plot between the drop radius R and the contact line speed dR/dt , both normalized to their values at 5 seconds. The plot showed a quantitatively

similar behavior for all the substrates where three characteristic stages for spreading were distinguished. The first and last have a slope of -2.5 and -4.5, respectively, while the slope of the middle stage was slightly positive as can be seen in Figure (5). It is worth noting that according to de Gennes [41], the slope of the first and last stage should be around 3.

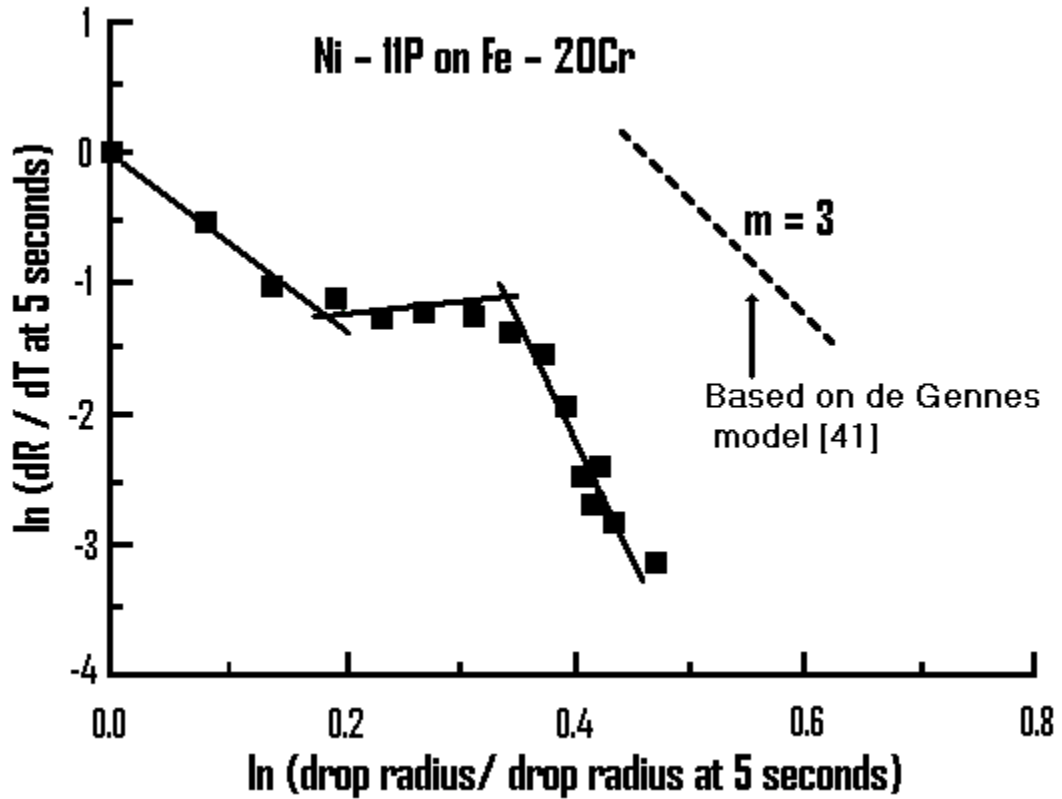


Figure 5 The change of the characteristic velocity of the brazing filler (redrawn based on Ambrose et al. [79]).

The deviation of the slope of the first and the last stages (when the system is considered microstructurally stable) from de Gennes [41] model was justified by the change of the liquid volume resulted from the substrate dissolution. The middle stage is related to the production of a new phase at the interface. This stage did not show a power law behavior but the data were fitted empirically by an exponential relation. The authors showed that this relation is also successful to describe the behavior of some other systems from the

literature that encounter compound formation from the reaction of liquid metal with ceramic substrates. This led to believe that the proposed empirical equation may represent the characteristic behavior of broad class of liquid spreading where reaction occurs with the substrate. Even though de Gennes' [41] relationship was applied when the substrate was microstructurally stable, the work of Ambrose [80] showed that the spreading rates were by far slower than those predicted by de Gennes [41] model. Ambrose [80] suggested, based on the experimental observations, that oxide reduction by dissolution acted as an additional damping force.

In spite of the importance of the current work for modeling the spreading behavior of brazing alloys, it can be more important in characterizing the industrial process behavior.

2.1.5 Observations and motivation

It is important to realize that the most significant work of Schonhorn [34], Hoffman [37], Tanner [39], Lelah and Marmur [40] and Ambrose et al, [79] relied mostly on experimental curve fitting. At the same time, it is obvious from the work of Ambrose et al. [79] that the graphical representation of the brazing filler flow data displays well, the stages and trends of the brazing filler flow process, regardless of their real complexity. This representation can reveal the influence of the input parameter on the actual spreading behavior during the brazing process. This approach might lead to defining the exact window of operation for the process based on the dominant parameters.

The mean to monitor the brazing drop spreading in a real environment at high temperature with a redundant flexibility to change the process input parameters is needed. As the required equipment is not available commercially and it is usually customized for

the purpose, this work will be dedicated to the detailed design, construction and testing of an apparatus suitable to study wetting and spreading behavior at working condition similar to those used during brazing operations. During designing this equipment all the concerns and concepts in this chapter were taken into consideration (as will be discussed in chapter 3).

2.2 An overview of the experimental techniques

It is usual to find authors in the literature who emphasize on the lag of high temperature spreading experimental work than its low temperature counterpart [54]. It is quite logical to guess that the sensitivity of the process and the capital cost of the equipments increase with the increase of the temperature of the experiment. This becomes significant at elevated temperatures where controlling the atmosphere becomes complex and even challenging to a certain extent. At the same time, the material selection becomes critical where it has to account for temperature, atmosphere and reactivity challenges [81]. Two major approaches are used to monitor high temperature liquid spreading; the first is using a hot stage with an optical or scanning electron microscopy, the second is using a high temperature furnace with imaging capability [78, 82-88]. The first method can reach a higher magnification. High magnification is desirable in the experimental set-ups. However, it implies that the monitoring screen should be in close proximity to the sample which can lead to the condensation of vapors from the high temperature liquid on the colder monitoring screen. More than that, the optics and the monitoring screen should be able to tolerate the high temperature and the chamber should stay vacuum-tight at low and high temperatures [86].

In the following part, an overview of the equipments and techniques used to evaluate solder and brazing filler spreading, equilibrium contact angle and liquid metal surface tension will be presented. Different techniques can be found in the literature to evaluate spreading including transferred, dispensed and spreading drop methods. At the same time, equilibrium contact angle measured using Sessile drop and Wilhelmy plate methods, while sessile, confined, pendant, and oscillating-levitating drop methods used to measure the liquid surface tension [53, 78, 99]. Sessile and spreading drop methods are by far the most used due to their simplicity and ease of implementation. However, they are criticized to be affected by solid and liquid surface contamination during heating and the confusion between sample melting and spreading in early stages [53]. On the other hand, Wilhelmy plate is criticized to be measuring non-equilibrium contact angle and for this reason some researchers used the approach to measure the dynamic contact angle, but it also measures the force driven dynamic contact angle and bypasses the complexity of liquid contamination [13, 100]. The same criticism applies to the transferred and dispensed drop methods where the drop is driven at the beginning of the transfer by inertia. These methods are also blamed for the complexity of the approach and the fact that for reactive liquid metal, there can be interaction between the liquid and the drop dispensing mechanism [53]. In some cases, special techniques are used, like tilted drops and drop shearing by moving objects to measure the advancing and the receding contact angle. In other cases, the spreading of brazing filler in slits was monitored to resemble the actual brazing gap [101, 102].

In all of the techniques used in the literature, heating method was either resistive or inductive. While inductive heating is faster temperature control is easier and more accurate in resistive heating [103].

Imaging techniques varied from still photography, videography and flash videography and samples were illuminated by light or X ray [104, 105]. The contact angle and the spreading area use to be measured from the hard images at early times. This was replaced by specialized hardware for edge detection as a part of the video circuits and specialized software based on thresholding and other edge detection techniques in imaging software era [106].

Chapter 3 Apparatus

3.1 Design outline

The goal of this work is to build a testing facility that can satisfy the demanding conditions required to study the wetting behavior of elevated service temperature materials used for capillary joining process. The equipment should also provide the capability to monitor and record the spreading behavior of the brazing filler metal under precisely controlled experimental parameters.

The joining environment requirements for Inconel718 as substrate, which is considered as one of the brazing environment sensitive nickel superalloys because of its titanium contents, and nickel filler metal AWS BNi-2 are used as a reference for the apparatus design. Based on the properties of these materials the furnace hot zone maximum operation temperature is selected to be 1450°C (2642°F). This exceeds the melting temperature of the metalloids containing nickel brazing filler alloys which is in the range of 1000 to 1250°C (1832 to 2282°F) [3].

A pre-brazing vacuum stage is needed to bring the brazing chamber and the sample surrounding environment to vacuum of at least 1×10^{-5} torr before heating the sample. This brings the chamber to the range of the dry-down vacuum zone to allow the best possible removal of the adsorbed oxygen, moisture and the volatile organic compounds in appropriate time [107].

Precisely controlled flow and partial pressure of high purity argon are needed. This will allow the evaluation of the effect of argon partial pressure on the spreading behavior of brazing fillers. Where the brazing chamber partial pressure is a compromise between the

higher amount of atmosphere impurities, such as oxygen and water vapor, which result from the increase of the argon partial pressure and the evaporation of the volatile braze filler contents that result from the increase of the vacuum at the test temperature [68].

Sample insertion to the hot zone should take place after the required temperature has been reached to acquire rapid sample heating. This is needed to achieve high sample heating rate that results in limiting the diffusion of melting point depressant (MPD) from the braze filler toward the bulk or the surface of the substrate prior to the melting of the braze filler. Melting point depressant diffusion out of the brazing filler prior to spreading leads to MPD depletion of the sample. MPD depletion might cause isothermal solidification on the sample periphery which in turn entangles spreading [108].

The droplet diameter estimated to be between one and three millimeters, this should minimize the effect of gravity on spreading to a negligible limit, and the substrate is around one square centimeter.

An externally heated tube furnace with 1.5 inch (3.8 cm) tube diameter is found to be the best suggested fit considering the sample size and the requirements of environment control. The choice of a vacuum tight tube with standard vacuum flange end-caps for the hot zone is an easy to implement and affordable design. One of the end-caps should be connected to a viewing port within not more than 35 centimeters from the sample to enable the special optics to acquire the droplet image in the hot zone at an acceptable zoom to monitor the spreading phenomena. An illustration of the furnace design based on similar systems in the literature [68, 87, 89-98] is shown in Figure 6.

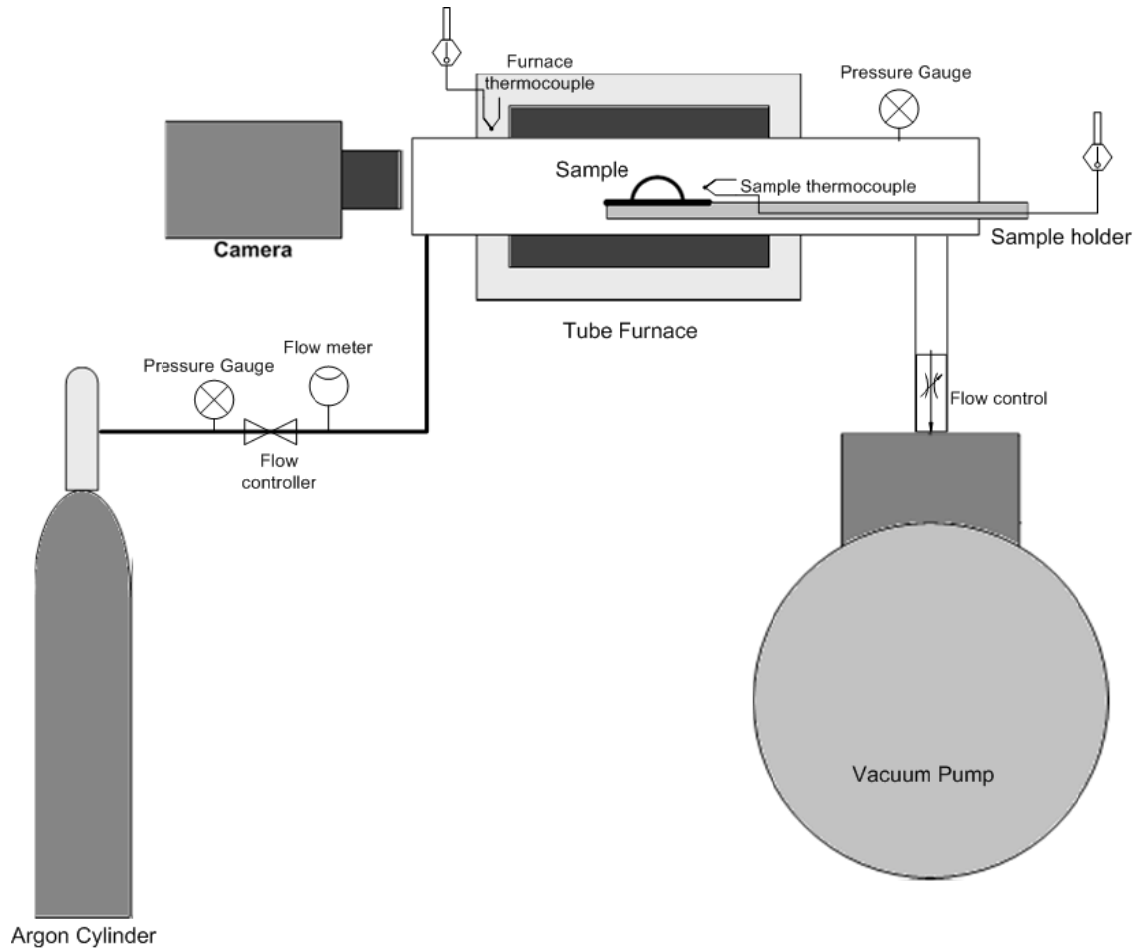


Figure 6 Schematic diagram for the wetting and spreading behaviour testing apparatus.

The need of the hot zone temperature to exceed 1250°C (2282°F) eliminates the use of Silica glass (fused quartz) for the furnace tube because its maximum operation temperature is 1200°C (2192°F) [109]. For the same reason, the use of K type thermocouple for the furnace temperature control is also eliminated as it can be accurately used for a maximum of 1250°C (2282°F). The need for an o-ring to connect the furnace tube to the vacuum end-caps impose that the temperature of the furnace tube ends does not exceed 200°C (392°F) in case of using Viton o-ring according to the manufacturer technical information. Because of the need to be as close as possible to

monitor the droplet and the limitation of the hot tube ends temperature, water cooling is needed for the furnace end sides.

The sample has to be transferred from the cold zone to the hot furnace core without breaking the vacuum, a special arrangement has to be done for this purpose. This will be discussed in more details later in the sample delivery subsystem section.

3.2 The apparatus subsystems

The described apparatus is composed of many components that perform different functionality either as a major contributor to the process or as a support for the other components. The apparatus design can be viewed as a collection of subsystems that are integrated to produce the desired performance and it can be sub-classified based on the different parts functionality as explained below:

- Furnace subsystem: This subsystem is responsible for heating the sample. It is composed of the heating core and the controller. The heating core is made to satisfy the dimensions and temperature requirements described in section (3.1).
- Vacuum subsystem: This subsystem is responsible for evacuating the system and to drive the argon flow. It is composed of two vacuum pumps, two pressure gauges, valves and standard vacuum connections.
- Argon subsystem: This subsystem is responsible for the control of the argon flow and ensures that the apparatus remains under controlled atmosphere throughout the entire test period. It is composed of an argon cylinder, different types of valves to isolate the different parts of the system and to control the flow, and mass flow controller.

- Water cooling subsystem: this support subsystem is necessary to the functionality of the furnace core and the diffusion pump as their operation requires water cooling. It is composed of valves, hoses, connections and a flow meter.
- Control subsystem: This subsystem is responsible for the sequence, the logic and operation of the different parts in the vacuum and argon subsystems. It is composed of two major control units and a pneumatic manifold in addition to the different sensors and the pneumatically controlled valves.
- Imaging subsystem: This subsystem is responsible for the sample illumination and image acquisition. It is composed of a high speed camera and an optics system including the lens assembly, illumination light source, a timer and an assembly holder.
- Sample delivery subsystem: This subsystem is responsible for moving the sample from the cold zone to the furnace core hot zone without breaking the vacuum, in addition to the sample temperature data acquisition. It is composed of a thermocouple and a temperature data logger and a vacuum feedthrough assembly.

The next section will explain the details of each subsystem.

3.3 The furnace subsystem

The furnace hot core and controller is designed and implemented by Thoughtventions Unlimited LLC according to the design requirements expressed in section 3.2. Detailed views of this subsystem are shown in Figures 7 to 12.

The furnace hot zone is enclosed inside a smooth alumina tube as it has a working temperature of 1600°C (2912°F) and its vapor pressure is around 7.6×10^{-7} at this temperature [110]. These properties of alumina made it suitable for the high temperature

operation and to tolerate the vacuum at that temperature. This alumina tube is suspended on two aluminum end blocks that are part of the furnace frame. The contact between the end blocks and the alumina tube is sealed with Viton o-ring. As the manufacturer (DuPont) recommended a maximum working temperature of 200°C (392°F) for Viton beyond which it releases toxic gases including hydrogen fluoride, the aluminum end blocks is water cooled by circulating water in a jacket inside these blocks as shown in figure 7.

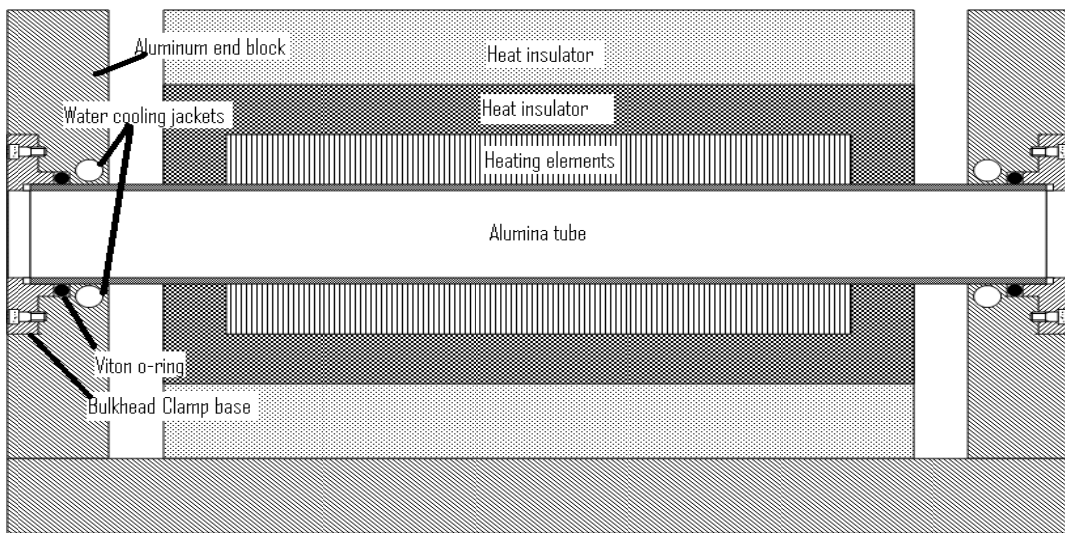


Figure 7 Illustration for the furnace hot core design

The alumina tube is externally heated using a 25 cm cylindrical silicon carbide heating element. As the SiC element has 1600°C (2912°F) maximum surface temperature, the use of the furnace is limited to 1450°C (2642°F) to prevent the oxidization of the element because oxidization is the main drawback of this type of elements [111].

The heating element is wrapped with two layers of insulator. The first layer is made of alumina bricks and the second is alumina wool. A small air gap is left between the aluminum end blocks and the heat insulators to allow the alumina tube to have some temperature gradient between the hot zone and the water cooled ends.

The alumina tube end in the aluminum blocks is interfaced on the opposite side of the aluminum end blocks with a standard bulkhead clamp base to allow standard interfacing with the vacuum and the argon subsystem as shown in Figures (8 and 9).

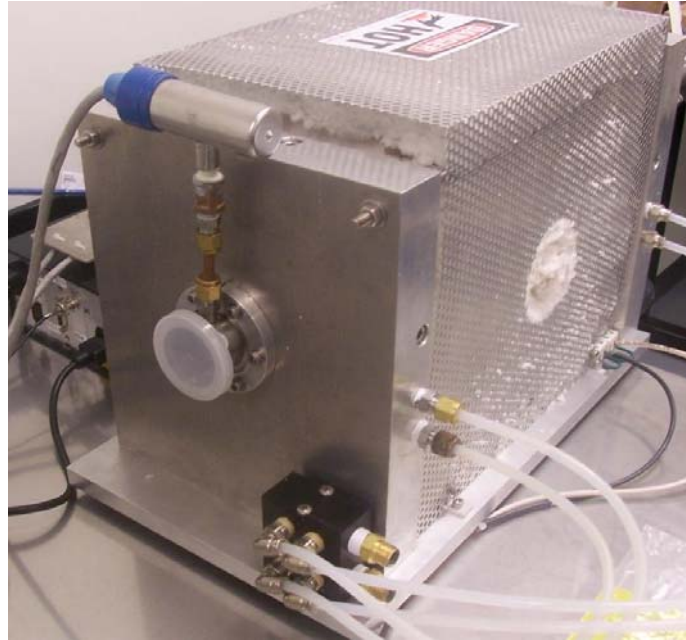


Figure 8 View of the furnace hot core

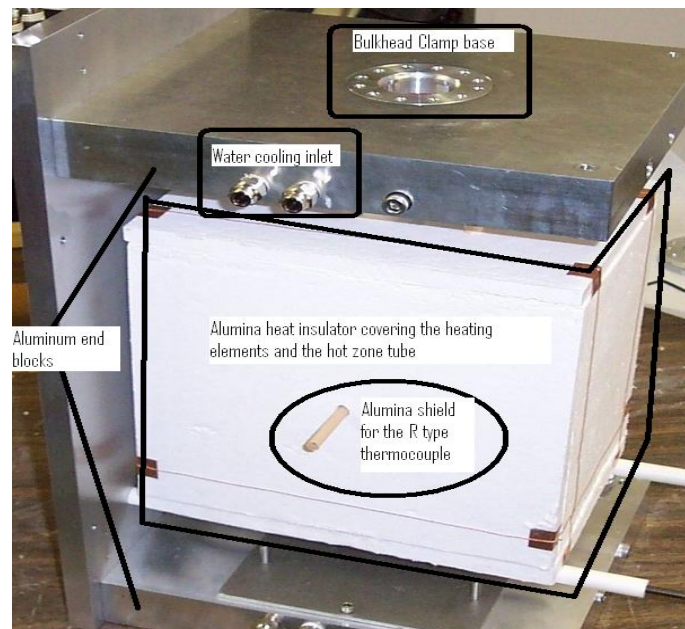


Figure 9 View of the furnace hot core during assembly

The heating process is controlled by a closed loop temperature control system to achieve a precise temperature control (See figures 10 to 12). This kind of temperature control requires a power controller to feed the heaters. As the resistance of silicon carbide heaters changes with aging and with temperature, a phase angle firing SCR power control with soft start and current limiting feature is used. These features allow smooth temperature ramping and prevent rapid element heating. This reduces the element oxidation and leads to longer element life. The power controller circuit is provided with a current limiting fast acting class T fuses to protect against elements short circuiting.

The silicon controlled rectifier receives a 4-20 mA signal from a panel programmable Proportional Integral Differential (PID) controller. This signal is based on a user set program and the feedback of an R type thermocouple to the SiC elements. This set-up gives a true proportioning control for the heating element temperature. The R type thermocouple is a platinum rhodium based thermocouple where it is known to be stable and suitable for high temperature measurements 1450°C (2642°F) with significantly reduced drift due to ageing and lower basic tolerance 0.25%. It is necessary here to stress that the furnace measured temperature represents the heating element temperature which might differ from the local temperature inside the tube. This imposes the necessity to measure the local sample temperature at the test time and to account for the variation when setting the furnace test temperature.

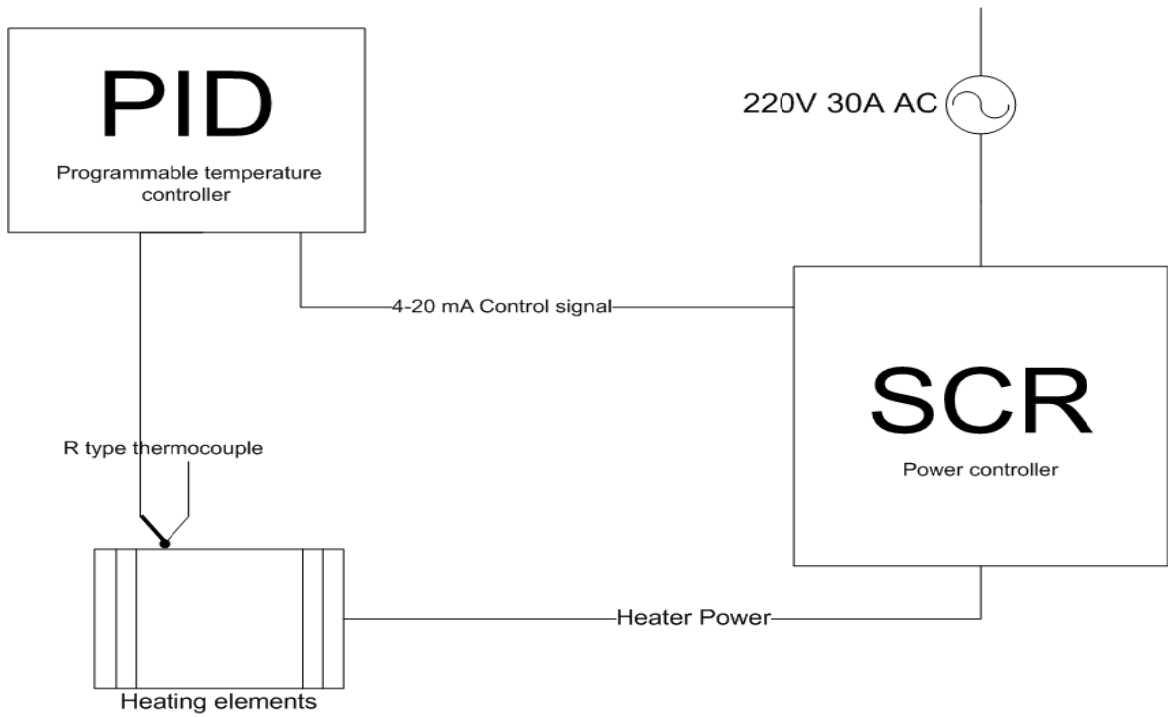


Figure 10 Illustration of the control circuit of the furnace



Figure 11 External view of the furnace controller

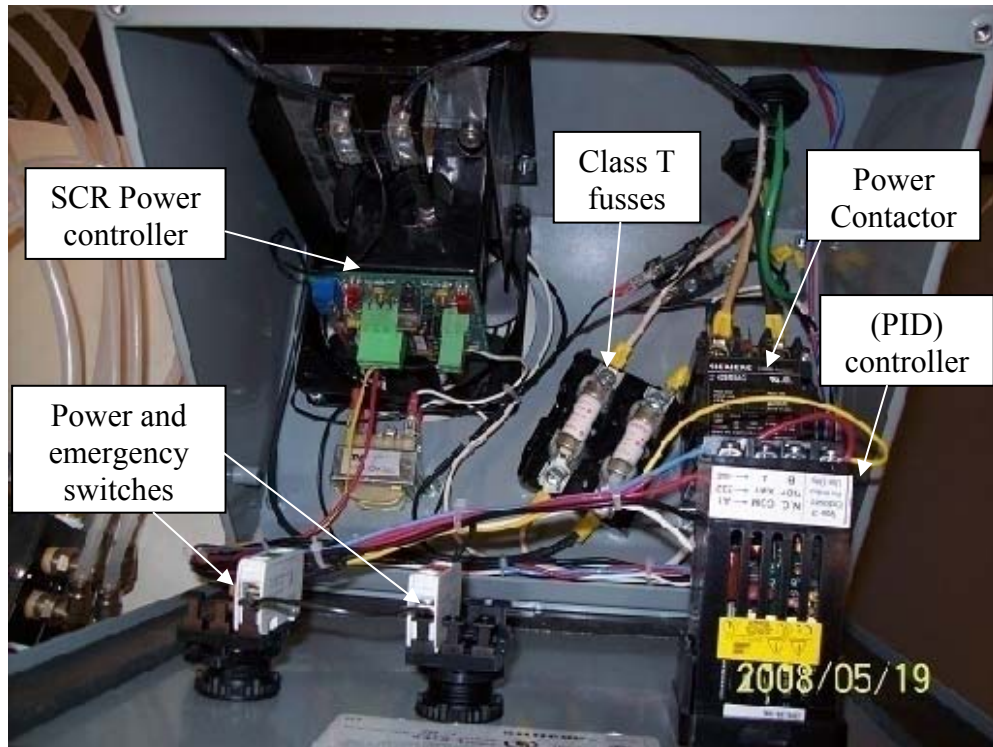


Figure 12 Internal view of the furnace controller

3.4 The vacuum subsystem

The vacuum subsystem has a dual role. The first is to circulate the argon under partial pressure. The second is to clean the sample and the environment around it by the removal of the undesirable adsorbants.

For argon circulation, the positive displacement oil sealed vane type rotary pump can drive the argon at the test desirable partial pressure and flow in a suitable cost. The use of this type of pumps can exceed the range of 10^{-4} torr but still its use is limited by oil vapor pressure at the operation temperature [112]. Exceeding the oil vapor pressure under molecular gas flow shall increase the rate of oil back streaming. Oil back stream is the major drawback of this type of pumps. The gas blast facility makes this choice more attractive where it allows the brazing paste to be dried in the same furnace prior to the test. Figure 13 shows the rotary pump used here.

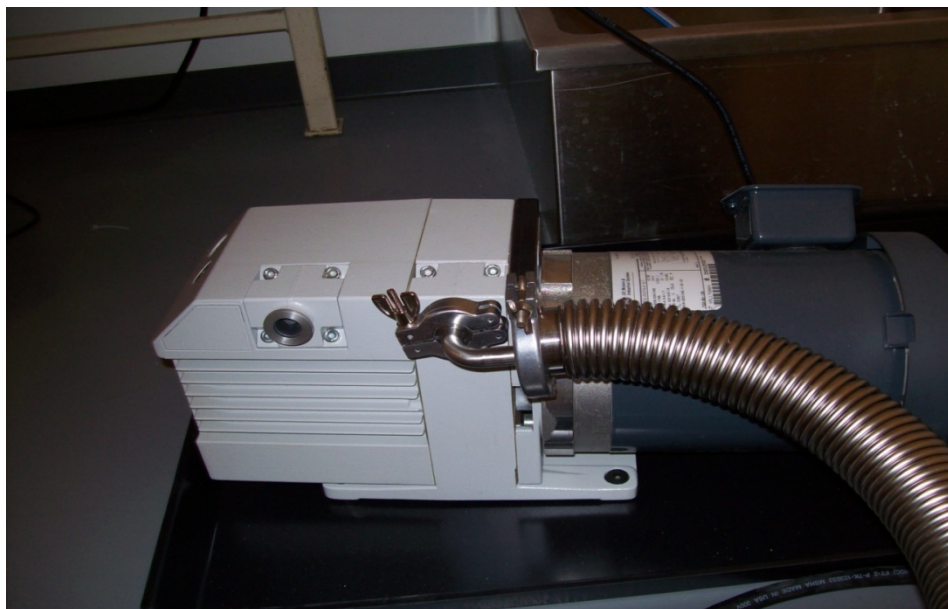


Figure 13 Rotary vane type pump used for rough vacuum

For the purpose of cleaning the sample from any adsorbed contaminants, the positive displacement oil sealed type pumps cannot handle the task satisfactorily. It is not recommended to run this pump in the molecular gas flow region [112]. The need for another displacement pump to handle this task practically narrows the choice between the vapor jet and the turbomolecular pumps. Because of the fact that the turbomolecular pump involves an accurate high speed moving parts, it is an expensive and maintenance demanding choice. The vapor jet, on the other hand, is simple and less expensive choice. However, using this kind of pumps is more demanding in control and operation. Generally speaking, vapor jet pumps are more favorable except in the processes that are very sensitive to oil contamination. In general, the regular level of oil contamination generated from the oil diffusion pump is deemed acceptable for many processes including brazing [113]. Based on this compromise the oil diffusion pump is used here for adsorbents cleaning. The diffusion pump used in the current work is shown in Figure 14.

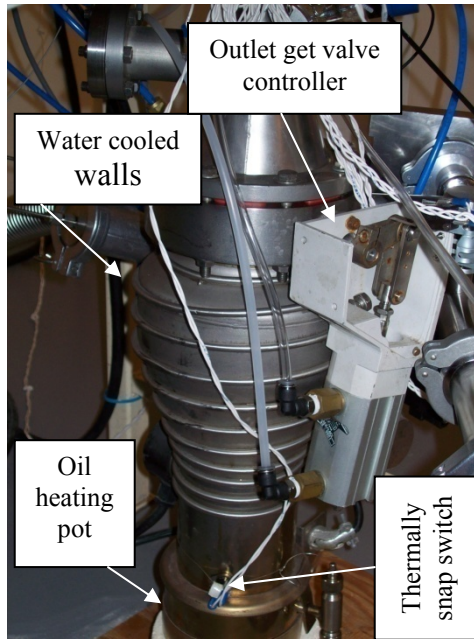


Figure 14 Oil diffusion pump used for deep vacuum

Even though the oil diffusion pump can perform up to a vacuum pressure lower than 10^{-12} torr, still the system ultimate vacuum pressure is dominated by the other components in the system. For the rough vacuum prior to the diffusion pump operation and to provide the required critical backing vacuum to operate the diffusion pump, the oil sealed vane type pump is used. This is the third role of the oil sealed vane type pump.

The triple role of the oil sealed rotary pump is managed through multi path layout controlled by valves and controllers. For backing the oil diffusion pump the foreline is linked to the rotary vane type pump via a line controlled by an isolation valve as seen in Figure 15. To handle the chamber rough vacuum, a roughing line linked the oil sealed rotary pump with the vacuum chamber. The flow through the roughing line controlled by isolation valve and butterfly throttle valve as can be seen in Figures 15 and 16. The throttle valve is used to differentiate between the foreline and chamber pressure. Figure 15 illustrate the complete system layout.

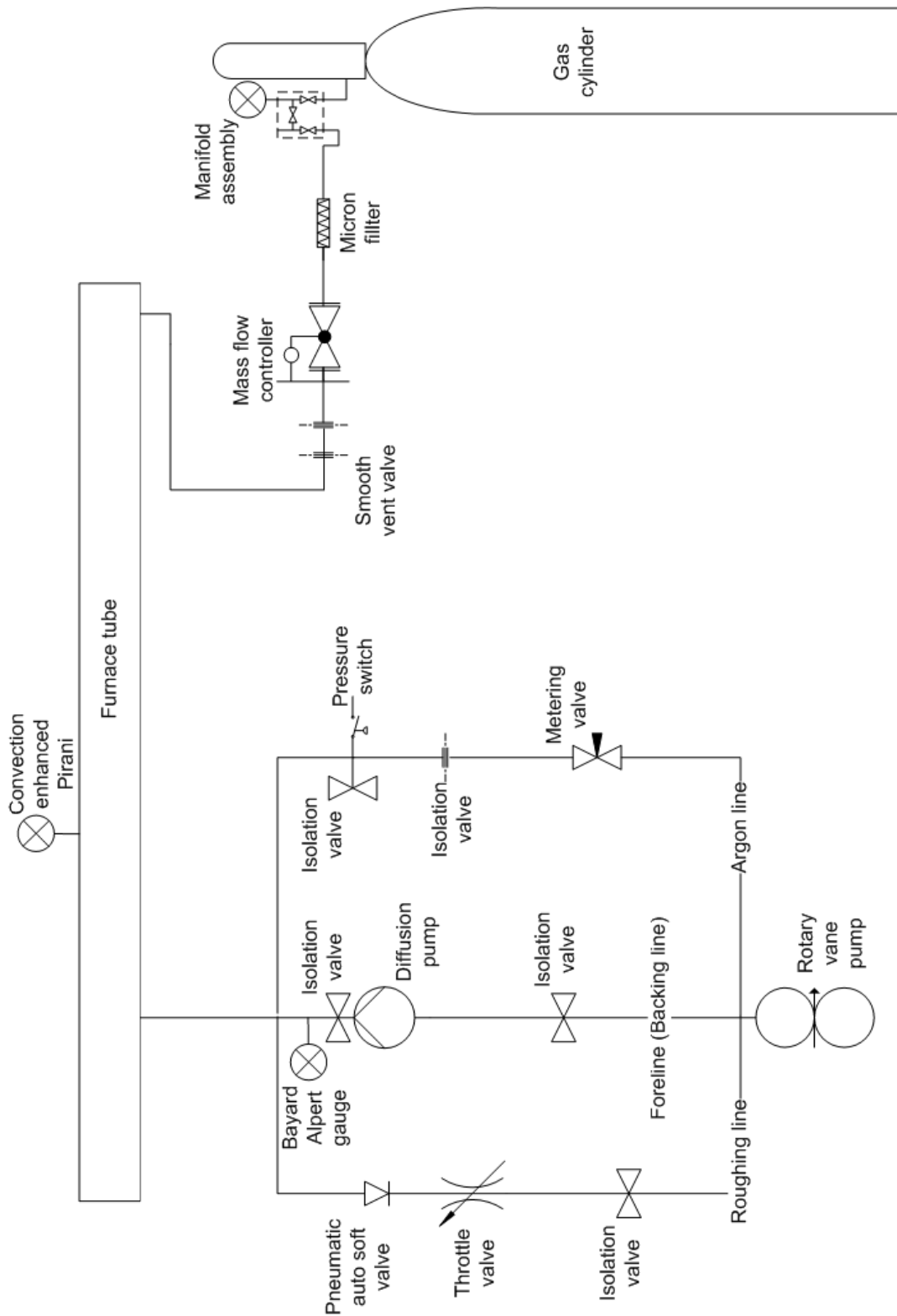


Figure 15 Schematic of the layout for the vacuum and argon subsystem

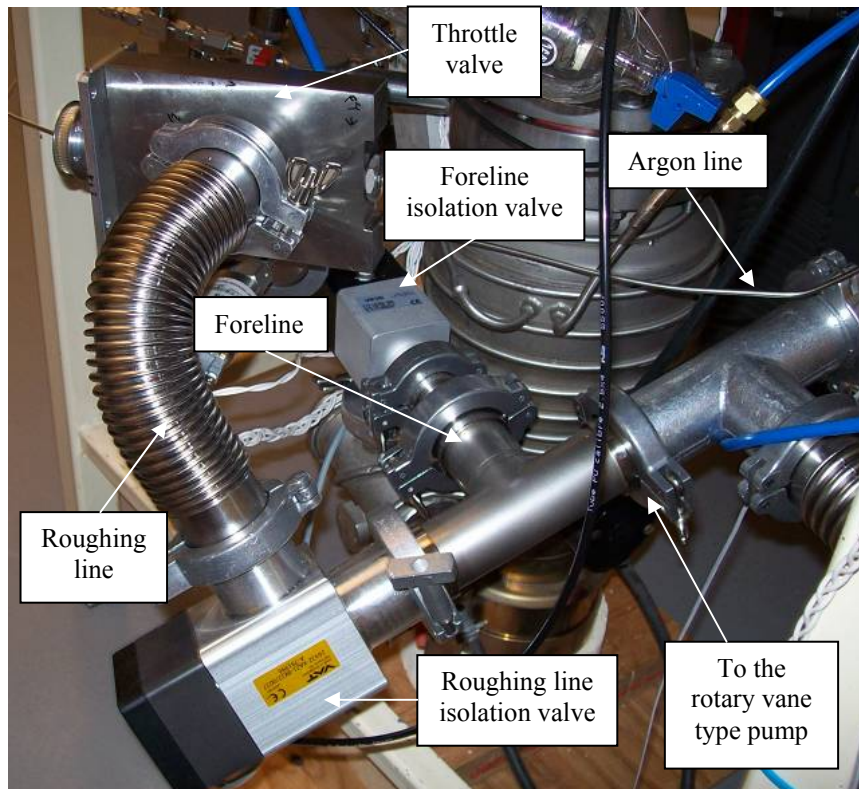


Figure 16 View of the vacuum subsystem tubing layout

To protect the vacuum chamber from the rotary pump oil contamination at high vacuum, the diffusion pump act as a seal against the rotary pump back streaming. However, it is still necessary to keep a slight flow of argon in the furnace chamber during rough vacuum. This argon flow should keep a viscous gas behavior in the furnace chamber to drift the back-streamed oil toward the pump [112]. As it is not recommended to start the diffusion pump when there is viscous gas flow at its inlet, the argon partial pressure has to be kept in the transition region between the viscous and the molecular flow. For this purpose, a manually controlled throttle valve is used on the roughing line to control the gas drift. A pneumatic auto soft valve is also used to protect the sample from being drifted at the beginning of the roughing process where a high gas flow rate is expected.

Stainless steel tubes and fittings are used to connect the different vacuum components and the furnace. These components are linked together using standard ISO quick flanges as shown in Figure 17.

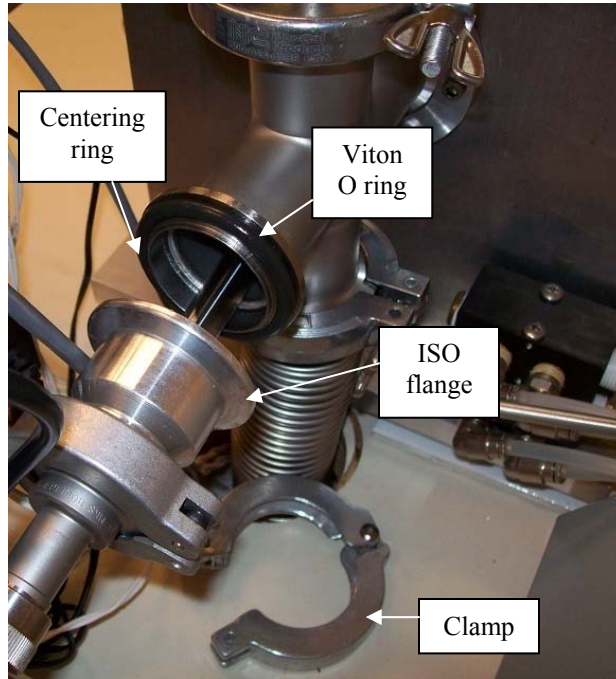


Figure 17 Standard ISO flanges used to connect between the vacuum components

The standard flanges are sealed using Viton O rings. The use of Viton in the flange assembly set the maximum vacuum in the range of 10^{-9} torr according to the manufacturer data sheets. This can be considered the theoretical ultimate vacuum pressure for this system. This limit is higher lower the practically expected pressure because of the different sources of out-gassing and virtual leaks epically the water adsorbed on the different internal walls of the system. Even though the system cannot be baked out due to the fact that many of the system components have a low baking temperature, still the system performance should be continuously enhanced with the use of the vacuum system. This expectation of performance enhancement with the system use

relies on the condition that the set-up has to be kept continuously under vacuum and it should be vented using dry argon rather than air.

To measure the chamber pressure and to control the vacuum subsystem operation, convection enhanced thermal conductivity vacuum gauge (Figure 18) is used.

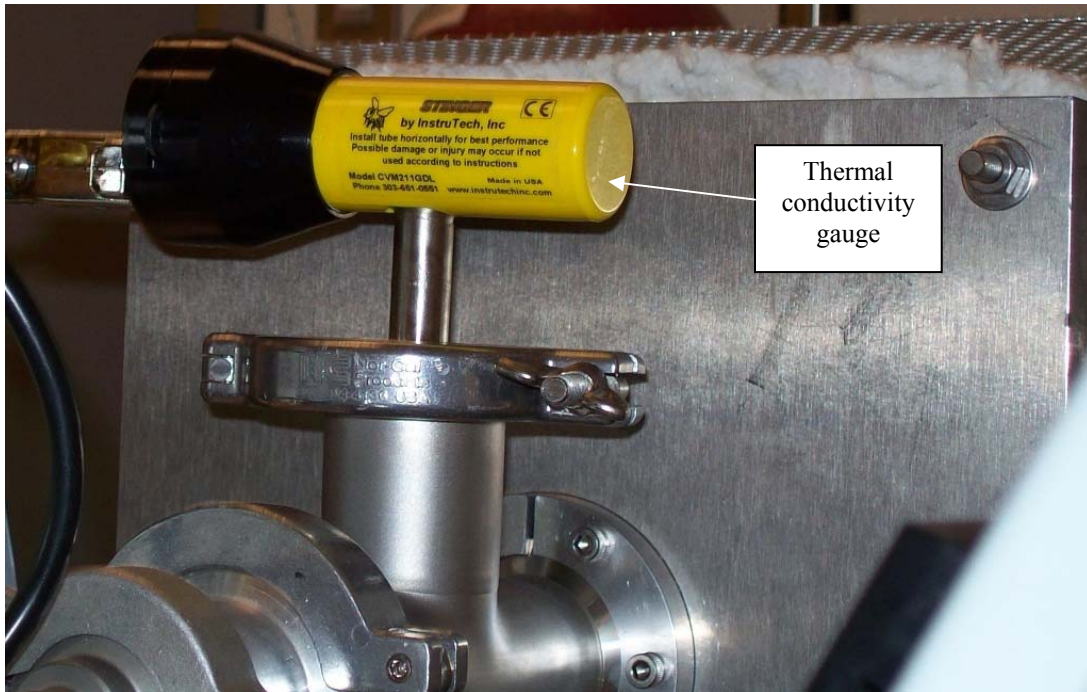


Figure 18 Convection enhanced Pirani gauge

For this type of gauge, it is important to keep in mind that for the range covered by sensing the gas convection (around 1 torr to atmospheric), the measurement accuracy is affected by the position of the gauge. The gauge should be positioned aligned to the horizontal axis. It is also important not to position this gauge in a hot environment as its principle is based on sensing the difference between the gauge hot filament temperature and the environment temperature [114]. The hot filament cooling rate is pressure and gas dependant where gases of different molecular size show different readings for the same pressure [114]. This is an important issue that should be considered when argon is used in this setup as the commercially available gauges, in general, are initially calibrated for air

or nitrogen use. When a thermal conductivity gauge that is filled with argon and calibrated with nitrogen, it will show a lower reading than argon actual pressure. This might lead to over pressurizing the chamber which can be considered as safety hazard [112].

To measure the vacuum pressure beyond the thermal conductivity gauge working range, an X-ray enhanced hot cathode ionization gauge (Bayard-Alpert) shown in Figure 19 is used.



Figure 19 X-ray enhanced hot cathode ionization gauge (Bayard-Alpert)

The gauge tungsten hot filament should not be exposed to a pressure more than 10^{-3} torr during operation. If the hot filament is exposed to air at a pressure higher than this limit, the filament will be oxidized. Because of the pumping effect in this type of gauge, degassing has to be done from time to time to ensure accurate gauge reading.

3.5 The argon subsystem

The argon is used to provide a dry inert test environment that satisfies the requirements of the brazing process and to support the vacuum subsystem operation. Precise control of

the gas flow and partial pressure provides the ability to test the effect of the process atmosphere dew point and the oxygen potential on the brazing process. Because of the argon flow subsystem and the vacuum subsystem act on the same furnace chamber, it is important for the argon subsystem to provide the required vacuum seal during the deep vacuum operation. As the argon is brought into the system using bottled gas, there is a possibility that the system might accidentally be exposed to positive pressure. Many of the components designed to work under vacuum and have a very limited tolerance to positive pressure. Precautions have to be taken not to allow positive pressure in the system. As the thermal conductivity gauge cannot be trusted for this task because its readings are gas dependant and because of its slow time response, a capacitance manometer pressure switch is used to trigger a valve that vents the system to the atmosphere if the chamber pressure exceeds 30 torr Gauge. The diaphragm manometers are independent of the gas type and have fast response [114].

For the sensitivity of the test materials to the atmosphere impurities, high purity argon is used. To keep the gas purity, rubber and polymer pipes and fittings are not appropriate in high purity gas handling where the gas can be contaminated from these materials themselves [8]. At the same time, copper tubes and fittings are not suitable to handle pressurized gas. All metal stainless steel tubes and fittings are used in this setup where the different parts are interconnected using VCR and compression fittings. As the gas handling components are used unbaked there is a possibility for the gas to be contaminated from the adsorbed water and oxygen on the inner walls of the pipes and fittings used to handle the gas. To reduce the effect of the gas contamination a micron filter used in the late stage of the gas handling. This micron filter reduces the amount of

the impurities in the gas up to 1 part per million according to the manufacturer specifications. This type of filters causes a high pressure drop in the line and limits the gas flow. This feature can be considered as an additional protection for the system from the cylinder pressure.

As the pressure drop in the system might vary with changing the valves settings and as the pressure drop in different parts of the system changes with the diameter of that part, thermal mass flow controller (0-50 standard cubic centimeters per minute (SCCM)) is used to control the gas flow in the system. This gives accuracy, flexibility and ease of control of the gas flow. Benefiting from the lairized input and output of the controller, a simple potentiometer is used to select the desired input portion of the maximum controller flow and a simple linear display used to display the measured flow. In spite of the possibility to connect the mass flow controller that is designed to function on vacuum system directly to the vacuum chamber, a smooth vent isolation valve is used in between as shown in Figure 20.

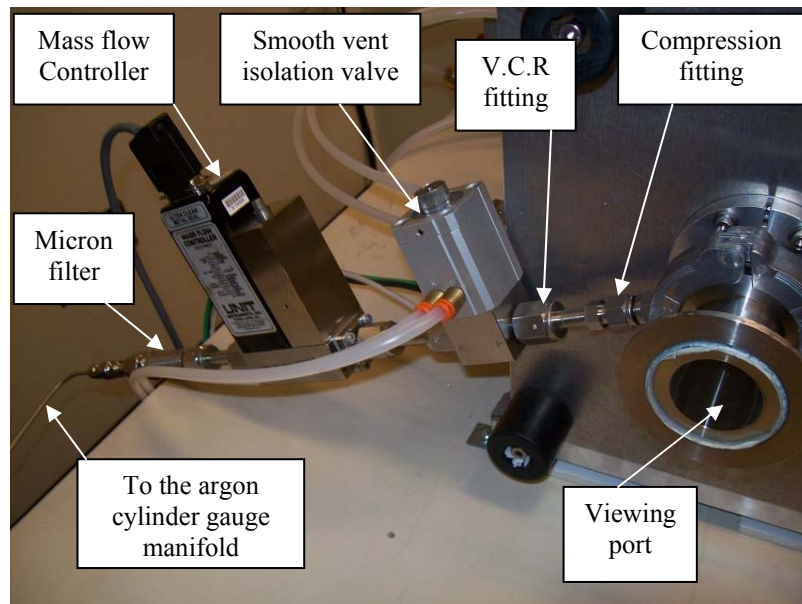


Figure 20 View of the argon inlet line

The use of the smooth vent valve allows the possibility to use many flow controllers together to act on the system. This arrangement gives the flexibility to expand the argon flow range and to mix different gases. The flexibility of mixing different gases accurately gives an opportunity to test the vacuum leak effect on the system and to test the fluxing effect of different gas mixtures.

To facilitate a more flexible pressure control at higher chamber pressure, a thin line used to pass the gas from the chamber to the mechanical pump. On this gas line, an isolation valve is used to seal the system during vacuum and a metering valve are (seen in Figure 15 and 21) used for precise flow control.

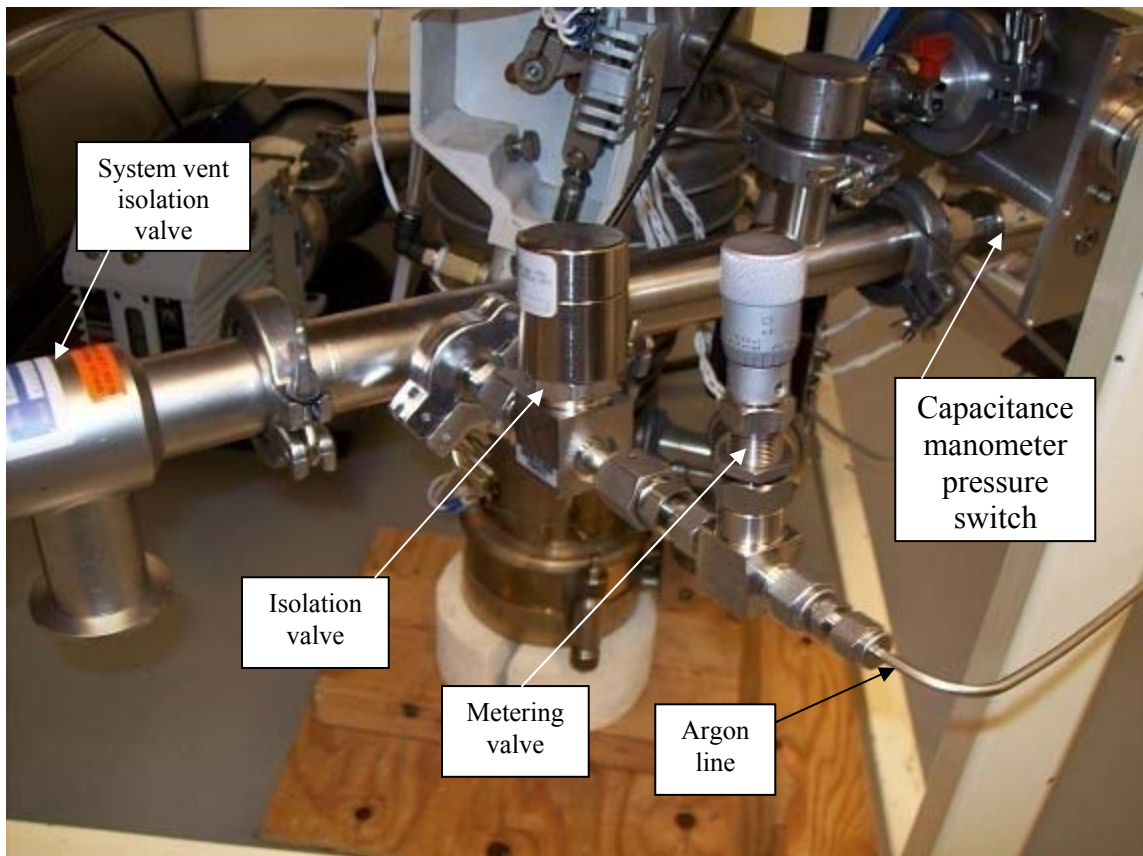


Figure 21 View of the argon exhaust and safety arrangements

3.6 The control subsystem

The operation of the vacuum and argon subsystems is fairly complex and requires a good attention against catastrophic failure that might end with system contamination or safety hazard. The control subsystem designed and implemented by the author to facilitate reasonable operation and to provide the necessary protections.

The control subsystem logic circuit and dash board is distributed in two control boxes shown in Figures 22 and 23.

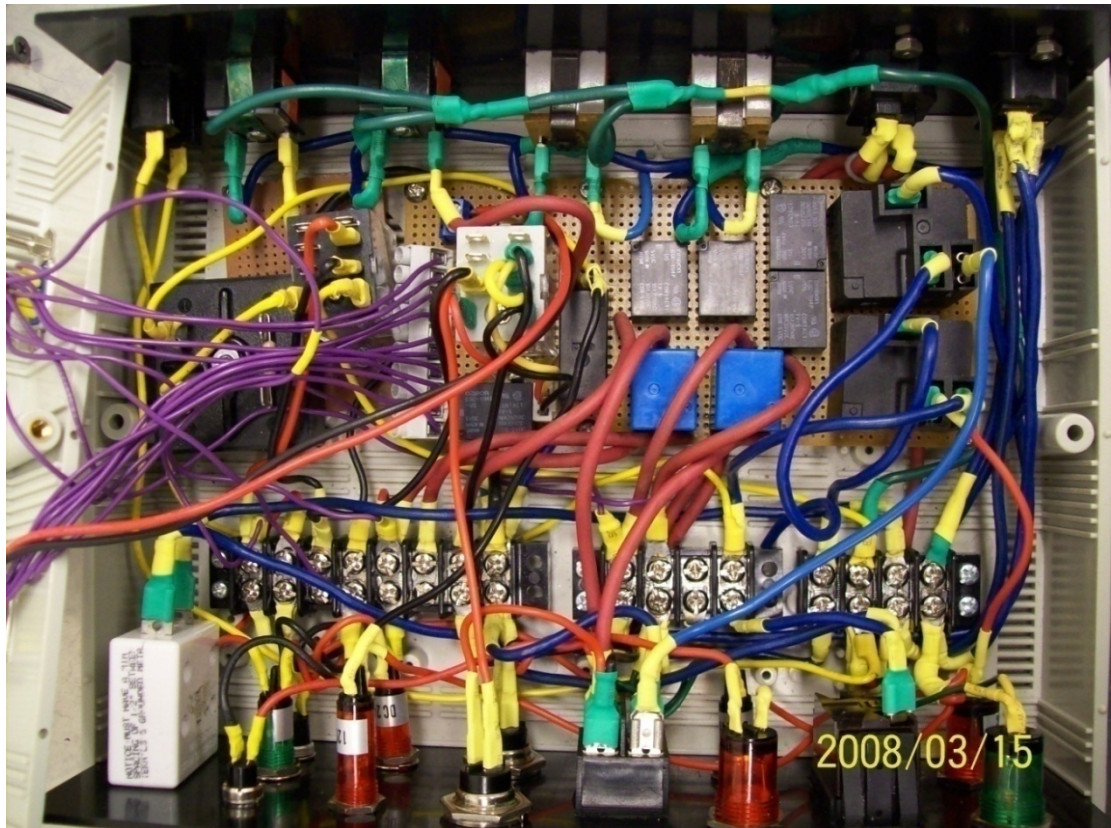


Figure 22 Control and communication board

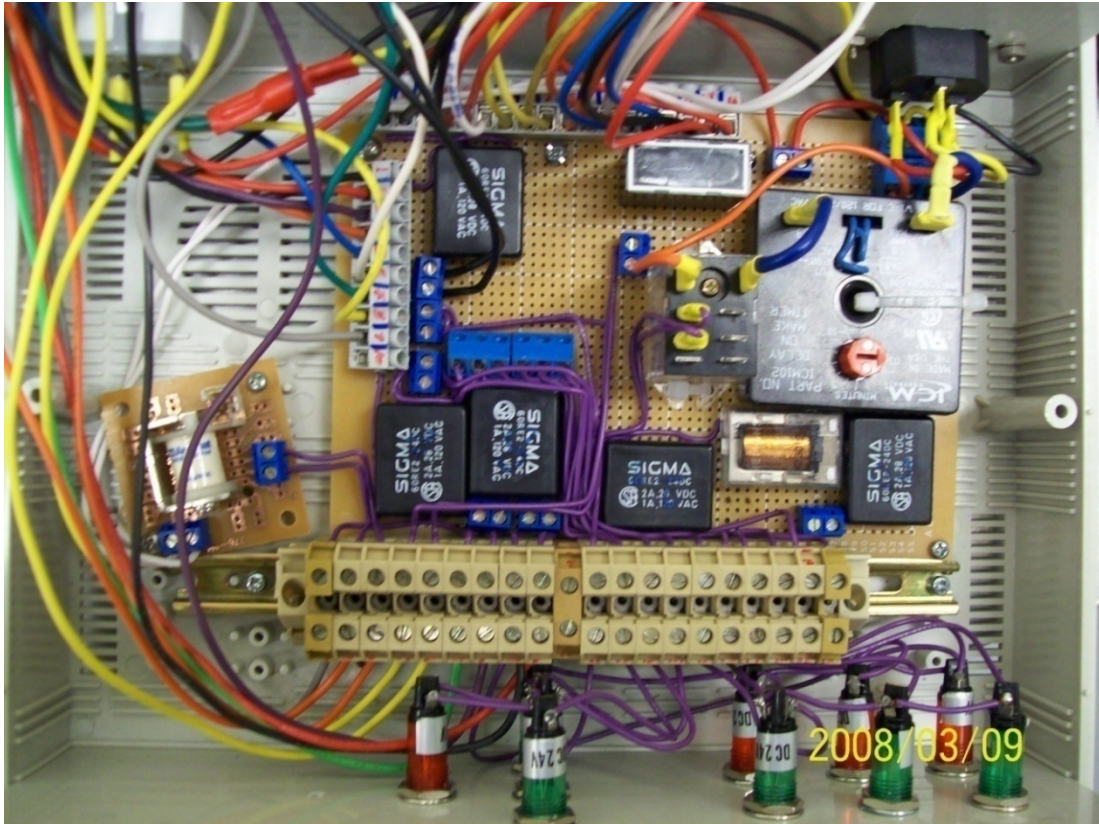


Figure 23 Valves and sensor synchronization board

The circuit can be operated manually based on user input, see Figure 24, or to be controlled using a digital signal from a computer or a microcontroller. The last feature made the whole apparatus readily computerizable.

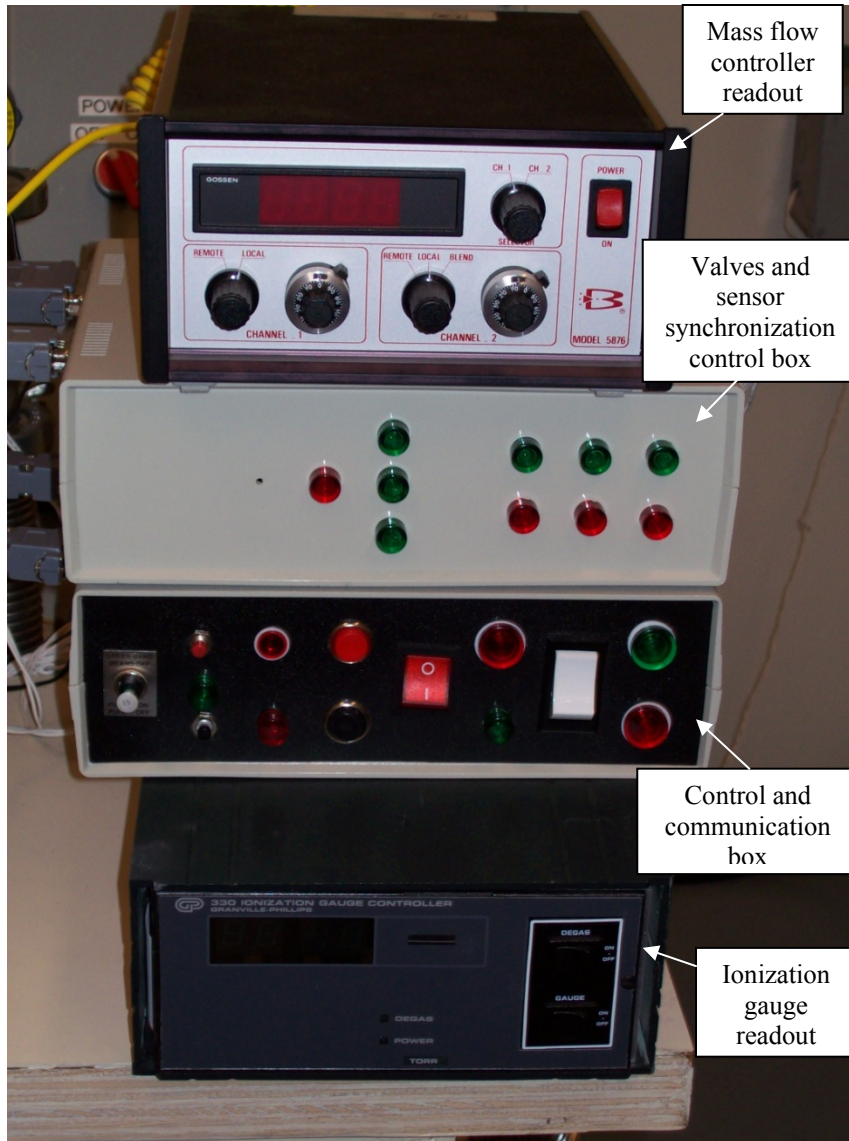


Figure 24 Control dash panel

Besides the user input the controllers receive different inputs from the sensors around the system. The behavior of the pumps and the different valves around the system results from the combination of these different inputs and the control circuit logic. The control circuit receives the feedback from the sensors and the valves indicators to assess the success or the failure of the process. All the isolation valves in the system are normally closed and pneumatically operated.

A 24 VDC pneumatic manifold handles the signal interfacing between the control circuit and the isolation valves. The tasks performed by the control subsystem can be explained based on the steps of system operation.

The requirements for rough vacuum are that the rotary vane type pump should be running and the roughing line isolation valve has to be opened. At the time the flow of the gas reaches the transition region between the viscous and the molecular flow, the argon flow should be started by opening the smooth vent valve. The high vacuum is divided into two operational steps. The first part is when the diffusion pump oil starts warming before reaching a fully developed jet. The second is when the jet is fully developed and the pumping starts. At the pre-developed jet operation the rotary pump has to keep roughing the furnace chamber besides backing-up the diffusion pump. This means that the backing and the roughing valves have to be open but the diffusion pump inlet valve has to stay closed. The argon flow should continue while the throttle valve has to differentiate between the chamber and the backing pressure. The high vacuum operation starts when the oil jet gets fully developed. The diffusion pump should handle evacuating the chamber at high vacuum with no argon flow while the rotary pump should keep backing the diffusion pump. For the high vacuum operation, the roughing valve and argon flow valve should be closed while the diffusion pump inlet and backing valves should be open. When the high vacuum operation end the chamber has to be filled with clean argon. This implies that when the diffusion pump stops and its inlet and outlet valves are closed the roughing valve has to stay closed not to have the air backfill the furnace through the rotary pump.

The argon flow pass through two different routes. At higher chamber pressure, the argon should flow through thin line for better pressure control. The isolation valve on the argon line should be opened while the isolation valves on the roughing line, the inlet and the outlet of the diffusion pump are kept closed. At lower chamber pressure, the argon passes through the roughing line by closing the valves on the argon thin line and the inlet and the outlet valves of the diffusion pump and opening the isolation valve on the roughing line.

The sensors and the feedback around the system distributed to fulfill the requirements of each step of the operation in terms of performance and protection. The rotary pump use for the roughing purpose is the first step of operation and does require any special control. As a protection for the system operator the three phase motor on the rotary pump gets operated through a contactor that receives 110 VAC signal from the control circuit.

An essential condition for the operation of the diffusion pump is that the backing pressure remains less than the critical backing pressure set by the manufacturer. This is monitored by the thermal conductivity gauge pressure switch and the foreline isolation valve feedback. Similarly the successful operation of the diffusion pump implies that the pump cooled walls temperature does not exceed the temperature defined by the manufacturer. Another important condition is that the oil boiler temperature does not exceed 200°C (392°F). These temperatures are monitored by thermally snap switches. All the mentioned conditions for the diffusion pump sound operation are guarded by the control circuit. The failure of any of them means that the diffusion pump will fail to start or will shut down and close the inlet and the outlet valves to prevent the contamination of chamber. To predict the right moment to switch from the diffusion pump pre-developed

jet operation to fully developed jet operation, the diffusion pump exit temperature has to meet the manufacturer specifications. This is monitored by a thermally snap switch. Another protection is added by setting a 10 minutes delay timer from the moment the pump starts till the opening of the pump inlet gate. When both of the conditions satisfied roughing line isolation valve will close and the diffusion pump inlet valve opens. To protect the diffusion pump inlet from being exposed to high pressure side, the pump inlet isolation valve is activated using the feedback signal from closing the roughing line isolation valve. To protect the diffusion pump from the argon high pressure, the argon circuit is deactivated by activating the diffusion pump inlet valve. To protect the ionization gauge from being exposed to high pressure the gauge power is activated by the thermal conductivity gauge relay signal. For the argon flow operation, the argon circuit is activated through the pressure switch relay and the diffusion pump inlet valve closed feedback.

For switching the system operation to computer mode, 5 volts relays are arranged in a way that can manipulate the panel operation and take over the system control. This is in addition to the fact that all the gauges and the controllers in the system accept 0-5 volt signal or have a 0-5 volt output.

3.7 The imaging subsystem

The main role of the imaging subsystem is to monitor the braze filler behavior during spreading. Also, it can be used for sample thermocouple calibration and to estimate the thermocouple time lag by monitoring samples that possess a well known melting temperature.

As the furnace tube diameter is 1.5 inch (3.8 cm) and the sample width can be around 1 cm and the braze droplet diameter should be between 1 and 3 mm. The proposed field of view is 9X3 mm. The depth of field suitable for this scenario should be more than half of the diameter of the spread droplet. To monitor the braze droplet at a distance of 300 mm which came from the dimensions of the furnace, it is not easy to provide a large depth of field with a suitable resolution. For this reason, the depth of field of the commercially available lenses can be enough to monitor the droplet profile. As the initial stage of the spreading phenomena can happen in one tenth of a second, the camera required to monitor the phenomena should be fast enough to monitor its progress. The regular video cameras standard can be 25 or 30 fps and some can be 60 fps interlaced. To acquire higher frame rates a special machine vision camera is needed. As the imaging shutter speed increases the exposure time is reduced. The light collection efficiency of the lens depends on the numerical aperture and the exposure time. The numerical aperture is defined by the sample distance, the effective aperture and the resolution. As the braze filler spreading phenomenon occurs at elevated temperatures exceeding 1000°C, this means that the sample and its environment should be bright enough to overcome the challenges imposed by the distance and the imaging speed. However, the excess brightness of the sample surroundings might affect the image clarity and blur the edges of the sample. This effect can be more serious in the case of using a CCD sensor where it is well known about its light sensitivity and the blooming effect. For this reason, the COMS sensor can be a better choice for this application, where it has a high dynamic rate as its structure prevents blooming, in spite of its reduced light sensitivity.

Taking into account all the details mentioned above, the imaging subsystem is built from the following components. A stand alone high speed (25 – 250 fps) C-mount camera that has a 2/3 inch 8 bit COMS monochrome sensor. This camera has a 1280 X 1024 pixel array at 25 fps and 640 X 480 at 250 fps and provided with 512 MB of internal memory which can give 8.7 seconds of continuous recording at 250 fps. The camera has an LCD view finder with a panel trigger as well as a USB view finder interface that allows computer trigger. The camera can accept contact closer or TTL signal for synchronization and trigger. The trigger starts recording till the memory gets filled or recording is interrupted keeping whatever recorded in the memory. This gives the flexibility to trigger after seeing the action on the viewfinder. A telecentric 1X fix magnification lens is used with this camera. This can give a field of view of 9X9 mm at the distance of 305 and a depth of field of 1.82 mm and a resolution of 0.015mm. To reduce the effect of vibration on the image the lens is mounted on a heavy holder that allows flexible position and direction adjustments. A variable intensity halogen light source with a flexible fiber optic extension is used to illuminate the sample during the sample adjustments prior to heating where the sample is not bright at that period. As the coaxial illumination affects the light collection efficiency of the lens, a side mounted illumination used in spite of the space limitation in front of the furnace tube as can be seen in Figure 25.

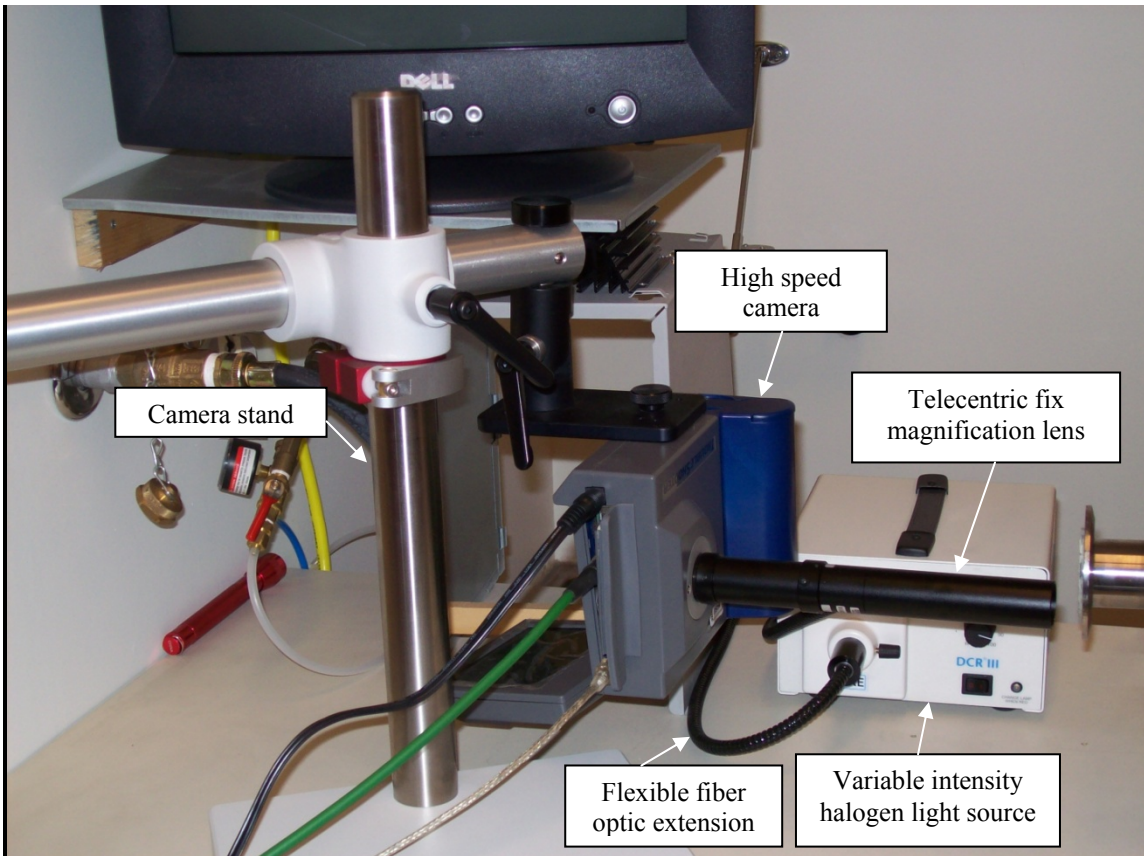


Figure 25 View of the imaging subsystem

3.8 The sample delivery subsystem

To achieve the highest possible sample heating rate, a mechanism that allows introducing the sample in to the furnace after reaching the set temperature without disturbing the vacuum is added. This mechanism also allows attaching a thermocouple to the sample to acquire the most accurate heating rate and local temperature. An additional benefit can be taken from this assembly is predicting the furnace temperature profile to have an exact expectation about its performance.

This mechanism is simply a Viton o ring sealed compression flange and a ½ inch (1.3 cm) stainless steel tube slides through it. Inside the tube, a K type thermocouple probe with an inconel 600 clad passes in the furnace. The stainless steel tube and the Inconel

clad are sealed together using stainless steel compression fittings. An Inconel 600 plate is welded on top of the thermocouple cladding to be the sample platform as can be seen in Figure 26.

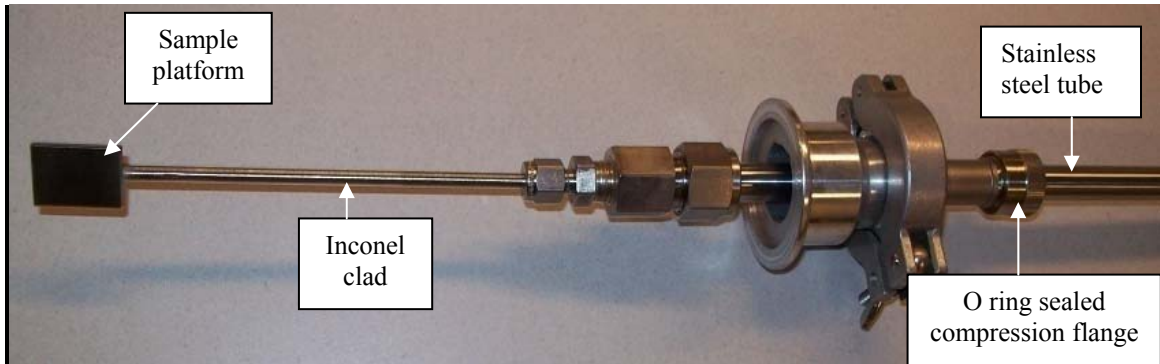


Figure 26 View of the sample delivery assembly

This assembly should not be used beyond 1150°C according to the manufacturer specifications.

As it is not possible to use the exposed type thermocouple to avoid breaking the vacuum, also, it is not preferred to use the grounded thermocouple because of the possibility for signal interference. Hence, an ungrounded thermocouple is used. The use of the ungrounded thermocouple type imposes limited time delay in the thermocouple measurements. A USB thermocouple data logger with a temperature update rate of 30 Hz is used for temperature acquisition.

Chapter 4 Testing and Measurements

The efforts summarized in the previous chapter were focused on the design and the implementation of the desired facility. These efforts ended successfully in constructing the test facility shown in Figure 27.

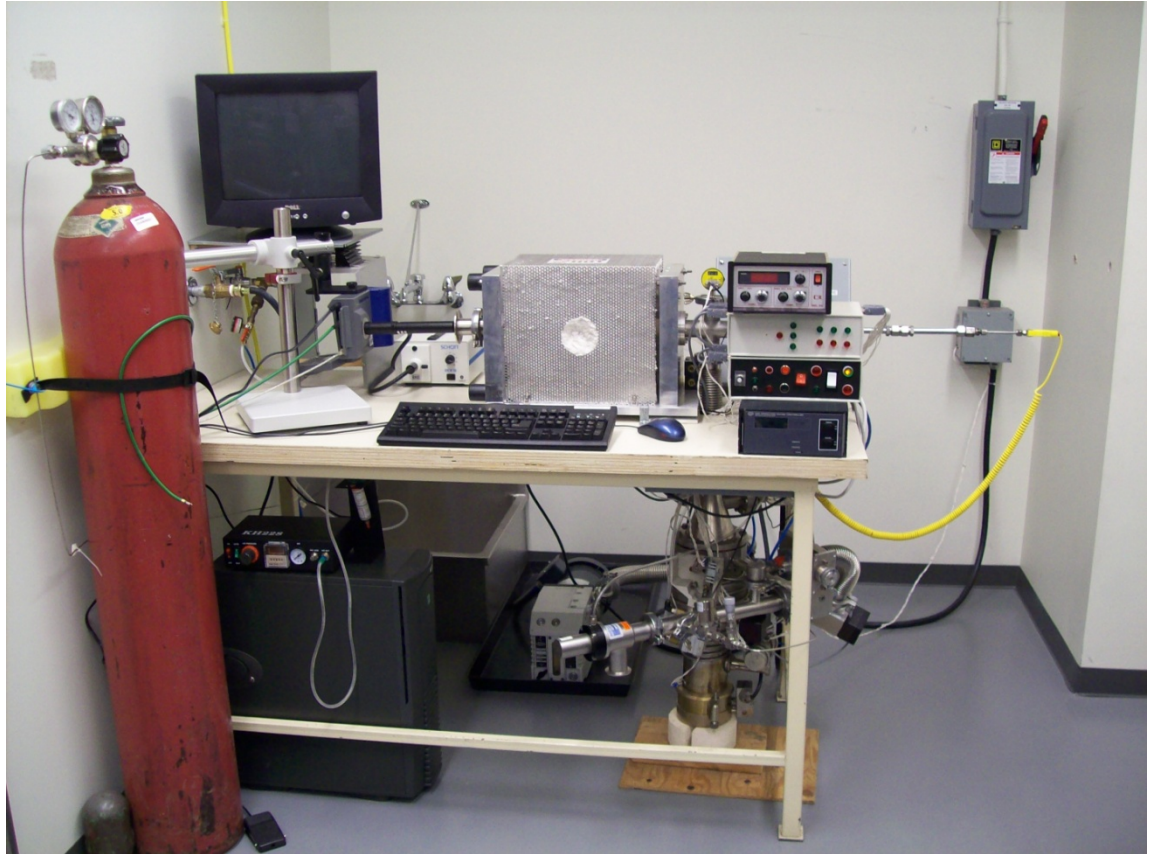


Figure 27 View of the complete facility to monitor the spreading behaviour of the brazing filler metals at high temperature

This chapter will be focused on testing the essential functions of this equipment and the type of data obtained using it. For the description of the control panel functions and some preliminary guide lines for operation see appendix A.

As the essential design requirement of the heating subsystem is the capability to operate at high temperature up to 1400°C (2552°F), the furnace hot core was tested successfully

at 1450°C (2642°F) for long time. However this temperature is near the ultimate limit of some of the materials used in this setup. Hence, continuous operation of the equipment at this temperature is not recommended, because it may cause fast ageing of these materials. Nevertheless, this equipment is not intended to be used as a standalone furnace and in most cases the sample delivery system, which is limited to 1200°C (2192°F) maximum temperature, will be used. If testing at higher temperature is required, the sample delivery system must be upgraded. Figure 28 shows the heating panel during operation.

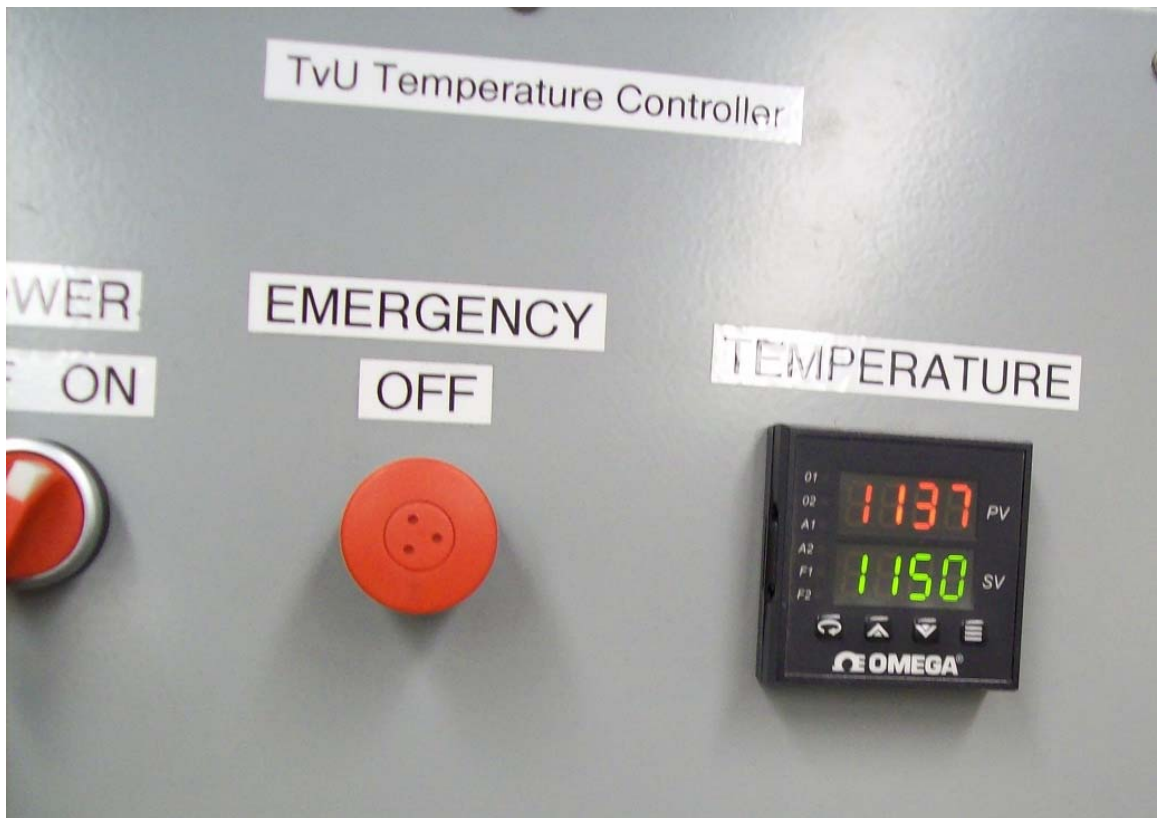


Figure 28 View of the heating panel during operation

The test of the vacuum operation showed that the system is leak tight. It is important to note that degassing occurs after quite a long time from the starting point (8 hours) which may appear as a leak in the system. This degassing is due to the residual humidity on the inner walls of the system components. The degassing was dramatically decreased by

keeping the system continuously under vacuum. On the other hand, the test of the vacuum operation showed a sound and successful operation of the related controllers which kept the system functional and fault free during the operations. It was possible to keep the system under vacuum in the range of 10^{-7} torr as shown in Figure 29.



Figure 29 View of the vacuum control panel during operation

The test of the argon flow showed stability for wide range of operation and precise control of the argon flow rate and the chamber partial pressure. The gas flow was controllable up to 10^4 division of the mass flow meter full range (50 standard cubic centimeters per minute SCCM); while the partial pressure was controllable in 0.01 torr steps as shown in Figure 30.



Figure 30 View of the argon subsystem during operation

Testing the imaging subsystem showed the ability to observe small objects at low temperature down to room temperature, where the sample was illuminated using the coaxial light source. Operating at low temperature is more difficult because at high temperatures the sample is emitting light. Figure 31 shows an image at room temperature for a 1 mm brazing filler drop with a resolution of 640X480 while figure 32 shows the same sample at 1100 °C. Both figures were acquired at the speed of 30 frames per second, at higher imaging speed the obtained image becomes darker and hard to be presented in printing.

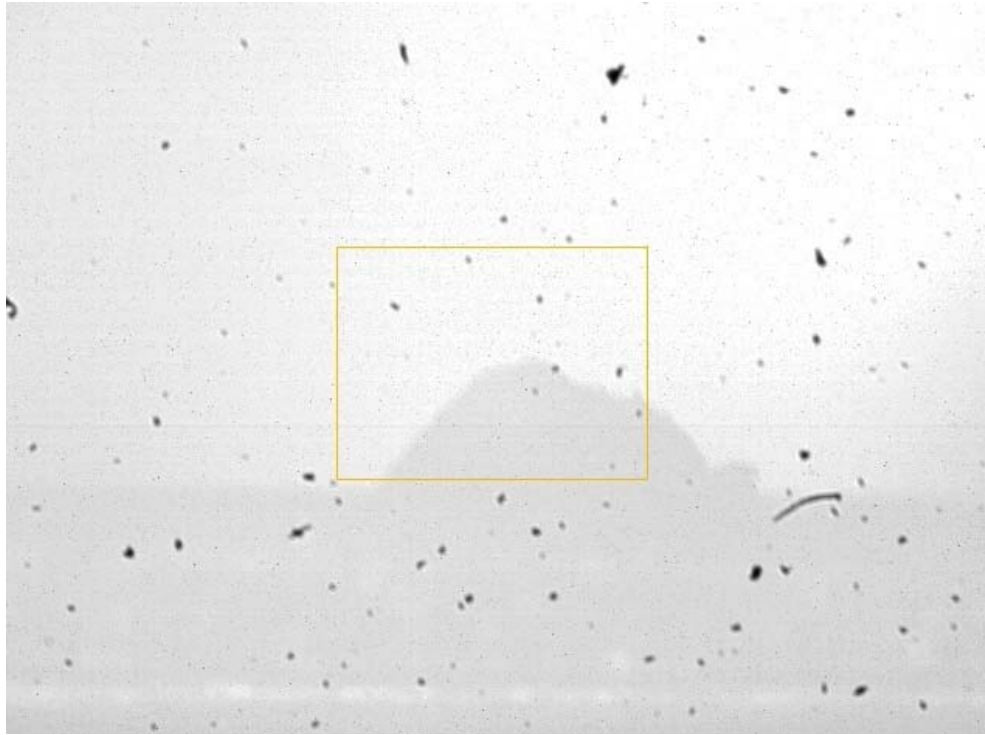


Figure 31 View of a 1 mm sample in the furnace at room temperature

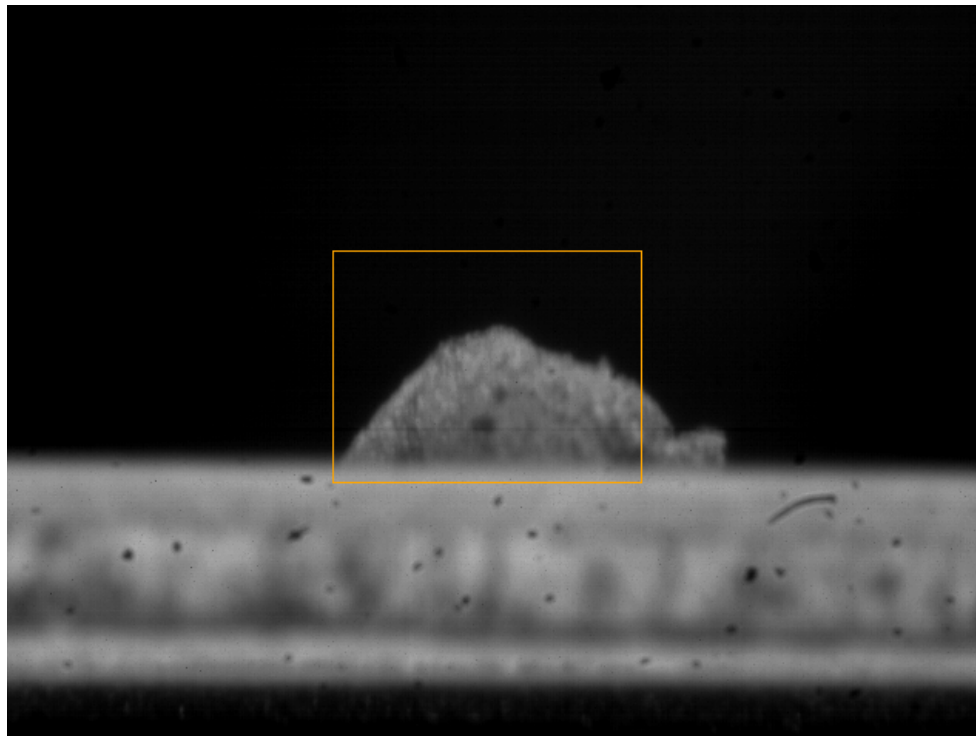


Figure 32 View of a 1 mm sample in the furnace at 1100°C

It was also possible to monitor the sample at 320X240 resolution as shown in Figure 33. This option increases the image acquisition duration which is limited by the camera's internal memory.

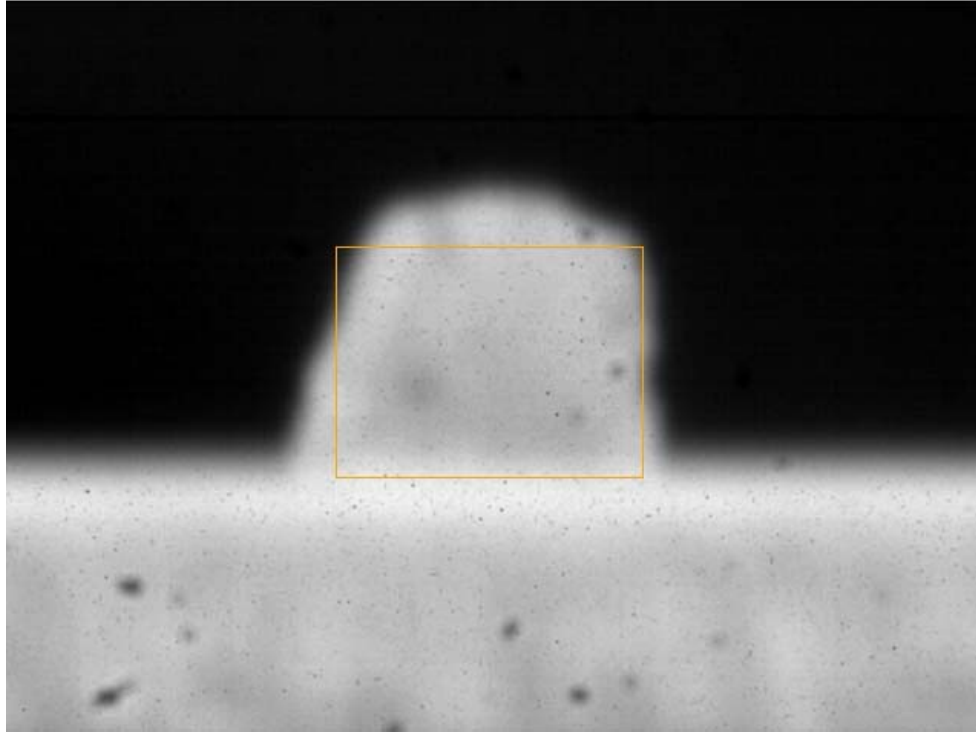


Figure 33 Image acquired at a lower resolution

As the basic function of the system has been tested and well established, the efforts are directed towards examining the potential output data. Few tests were conducted using different high temperature alloys like SS410, INCO625 and INCO718. As the target of the experiment is to examine the capabilities of the test facility rather than the material properties, there was no attention paid to the sample preparation requirements or the choice of the test atmosphere. In general, due to the use of COMS sensor, the large zoom and the high recording speed, the acquired images were relatively dark. When the imaging speed is very high, the images might be non-presentable and difficult to analyze. For this reason, digital image processing and analysis techniques are used to obtain

meaningful data out of the original images. To facilitate this task freeware programs have been used. VIPBase Program [115] has been used to break the video into images then these images were flipped upside down, thresholded, edge detected and inverted. This treatment ended in representing the substrate and the drop shape by an easy to analyze curve. Figure 34 shows the steps used in image analysis.

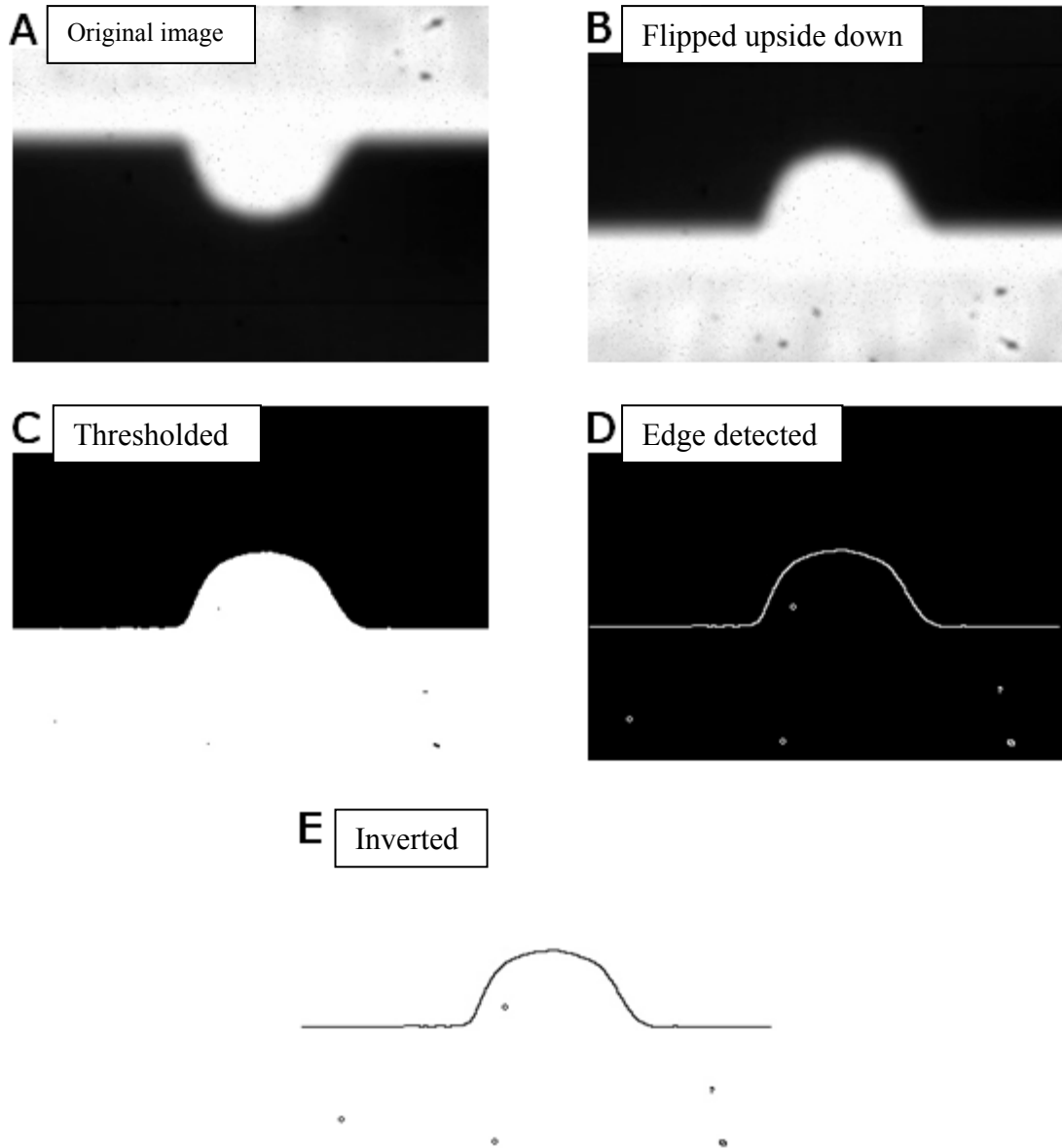


Figure 34 The steps used for image analysis

MB-Ruler [116] and SCALE 2.0 [117] programs have been used to measure the screen dimensions and the apparent contact angle for a selected set of images. The screen dimensions are certainly different than the real sample dimensions and there might be some distortion in the image aspect ratio. However, it is assumed that the distortion is constant through the image and it should not affect the frame to frame comparison. The relation between the screen measurements and the real dimensions can be established by the precise measurement of the droplet dimensions before and after the test.

It is important to note that the use of software for droplet measurements on the screen might end up confusing as the magnitude of on screen zoom used in a specific scenario might influence the extracted results. A good judgment is necessary for accurate measurements. In this work, the height of the droplet and the contact angle measurements were fairly manageable, whereas measuring the width of the droplet was more challenging. As the substrate in the digitally modified images is some time represented by a smooth line (see Figure 35) and in other times by more of a distorted line (see figure 36), it was not possible to conclude in any case if the difference is based on the existence of a thin layer of liquid or measurement artifact resulted from the image quality and/or the used image analysis technique.

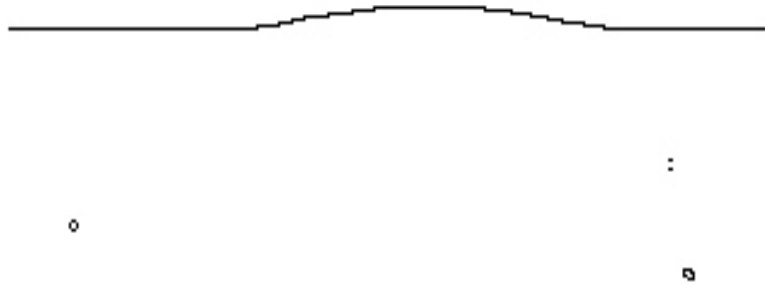


Figure 35 Example of a substrate represented by a smooth line

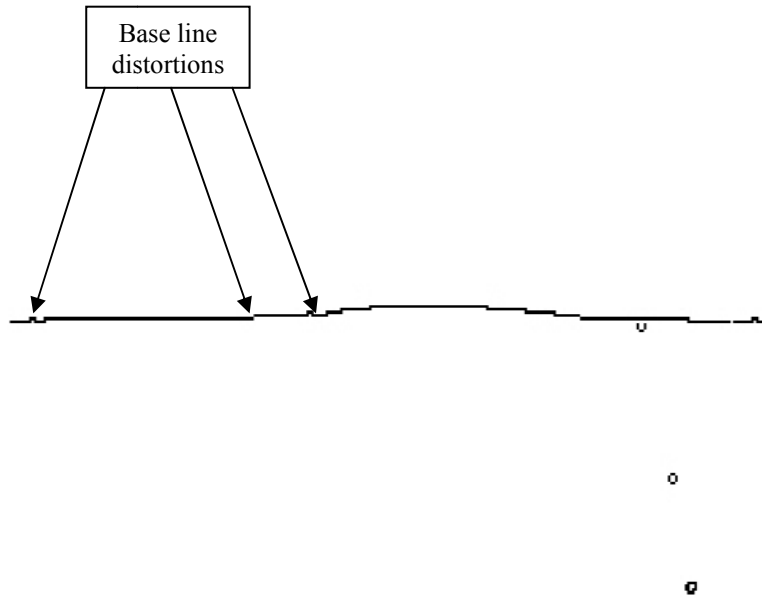


Figure 36 Example of a distorted substrate

This artifact can be caused by on one or more reasons such as the imaging analysis, the low imaging resolution, the vibration, the possible mismatch between the optical axis and the substrate plane and the optical illusion due to the glow and the illumination.

Chapter 5 Discussion, concluding remarks, contributions and future recommendations

5.1 Discussion

In this chapter, some basic issues concerning the observed spreading behavior will be highlighted and some elementary analysis will be carried out. The purpose here is to demonstrate the fitness of the test facility for monitoring the brazing filler spreading behavior.

The test of a large sample, 3.5 mm in diameter, showed a nonsymmetrical spreading that can be an indication of the influence of the liquid gravity on the wetting behavior. The acute contact angle in the direction of spreading indicated a capillary driven spreading, while the curvature of the liquid front indicated inertia inhibited spreading as the liquid still was sluggish at the beginning. Figure 37 shows an early stage of a large drop spreading.

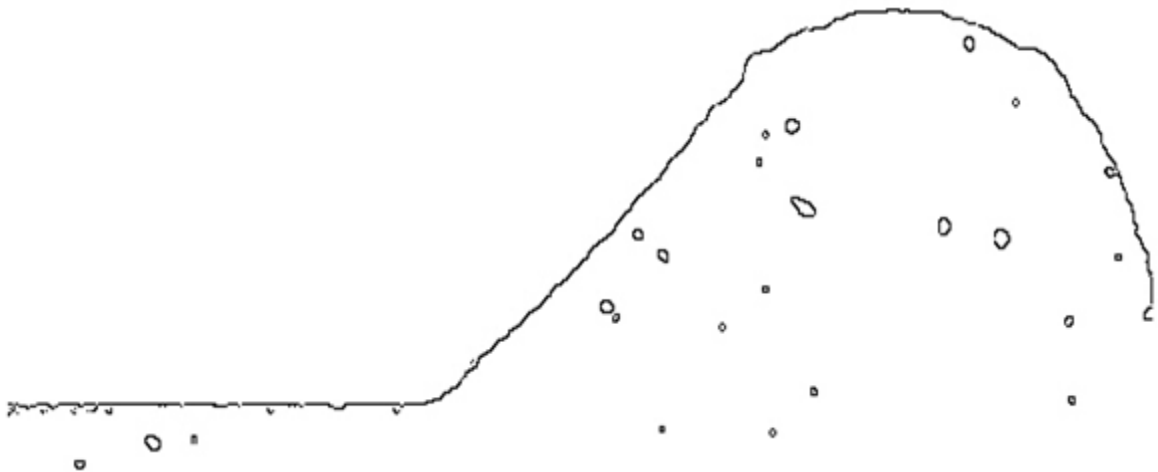


Figure 37 View of the spreading of a large drop hindered by inertia.

As melting is completed the flow of the liquid in the bulk of the drop resulted in inertia assisted spreading as it can be seen from the liquid front shape in figure 38.

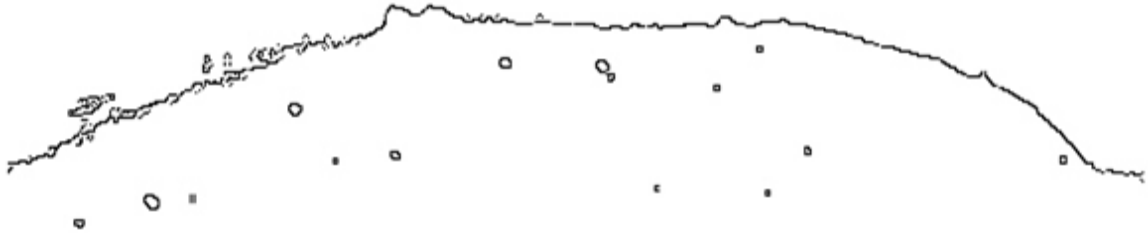


Figure 38 View of the spreading of a large drop assisted by inertia

Testing of a smaller droplet, 1 mm in diameter, shows a more uniform spreading which is an indication of the dominance of capillary forces on spreading as shown in Figure 33. The change in the droplet height, width, left contact angle and right contact angle with time for a selected number of frames measured and listed in table 1. As spreading starts with melting, there is a period where the changes in height and width start while the liquid surface still forming and not well defined. The contact angle in this period is designated by M in the table.

Frame No	Time (sec)	Height (mm)	Width (mm)	Width at 30% of the height	Left contact angle (°)	Right contact angle (°)
0	0	188	315	251	M 90	M 90
25	1	183	317	251	M 90	M 90
50	2	177	315	251	M 90	M 90
75	3	164	320	262	M 90	M 90
100	4	148	325	270	68	57
125	5	103	352	283	41	35
150	6	63	373	328	28	22
175	7	50	376	339	23	21
200	8	48	389	344	21	19
300	12	40	381	354	18	13
400	16	37	365	368	16	11
500	20	32	368	402	10	8
600	24	29	373	376	9	7
700	28	29	386	362	8	8
800	32	26	405	402	8	7
900	36	29	368	368	8	8
1000	40	24	413	413	7	7
1500	60	21	405	405	5	5
2000	80	21	362	362	4	4

Table 1 The data obtained from the analysis of the primary facility test results

The data in Table 1 are plotted against the time to examine the trend of change in each set. The drop height change with time, shown in Figure 39, indicates a clear dependence on time.

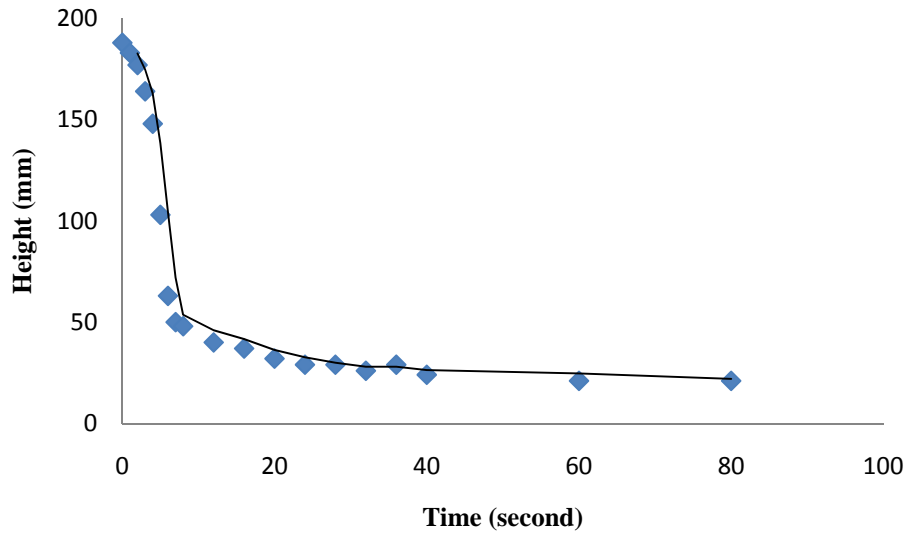


Figure 39 The change of the height of the brazing filler drop (measured from the magnified image) with time

The plot of the change of the drop base width with time started to show a clear trend at the beginning, till the drop height decreased to a level that influenced the measurements. From that point the scatter of the data dominated the curve, as shown in Figure 40.

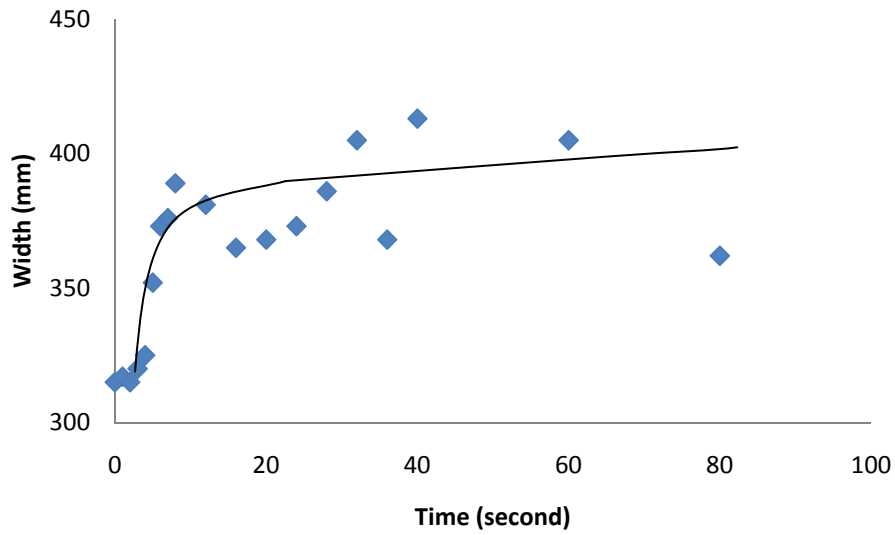


Figure 40 The change of the width of the brazing filler drop with (measured from the magnified image) time.

The plots of the contact angle change with time for the both sides are shown in Figures 41 and 42. Distinctive time dependant behaviour is observed, very similar to what had been seen for the drop height with time.

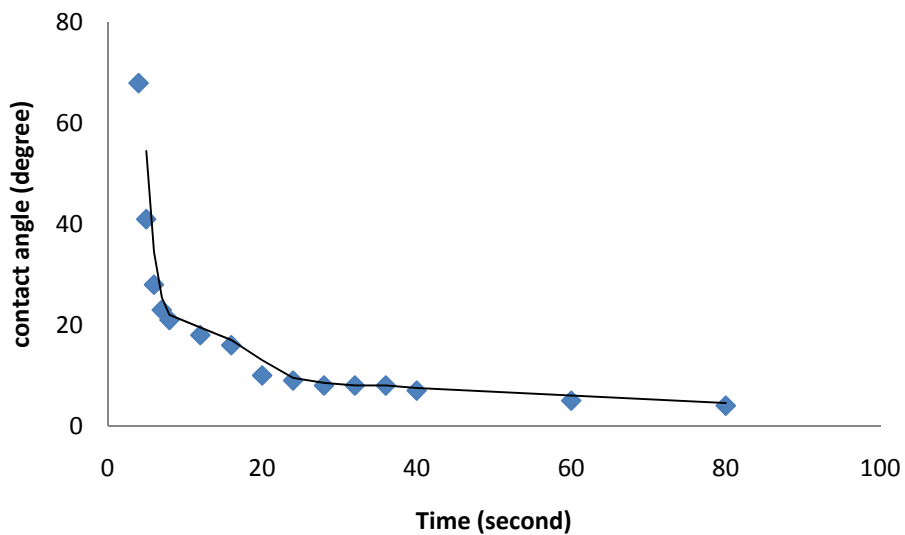


Figure 41 The change of the left contact angle with (measured from the magnified image) time.

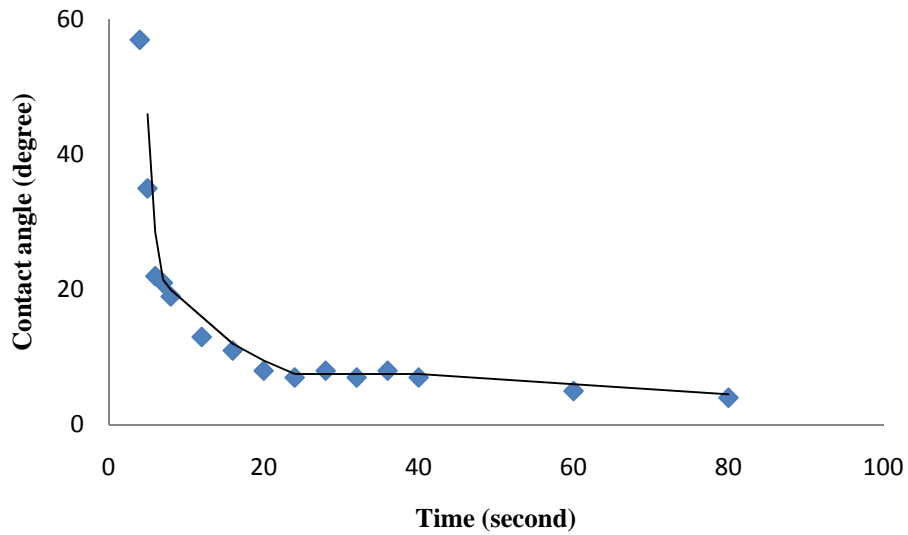


Figure 42 The change of the right contact angle with (measured from the magnified image) time.

To examine the three stages of spreading, the changes in the height and width of the liquid drop with time are plotted on a log-log diagram. The plot of the height against the time, see Figure 43, showed a clear three distinctive regions. In a very similar fashion to what had been reported by Ambrose et al. [79]. This behaviour is considered as a characteristic function of the spreading of a specific material at certain experimental conditions [79].

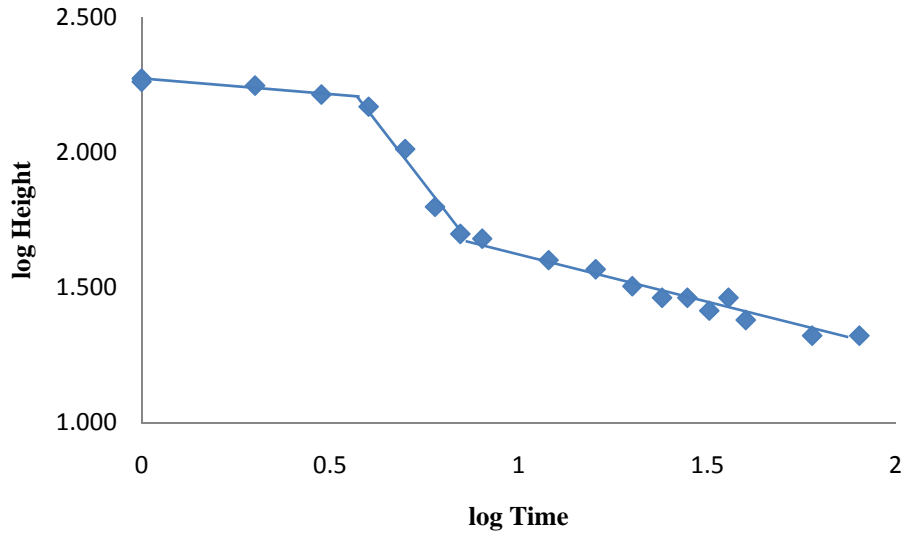


Figure 43 The plot of the change of the height of the drop with time on a log-log diagram.

The plot of the drop width change with time on a log-log diagram, Figure 44, shows the three-region trend, except the fact that the data in the third region are scattered due to the previously mentioned problem in measuring the width accurately.

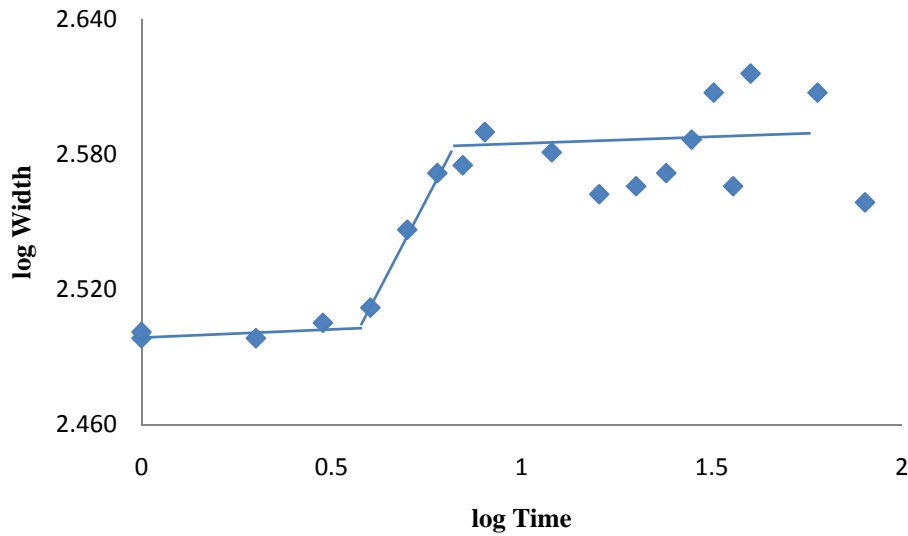


Figure 44 The plot of the change of the width of the drop with time on a log-log diagram.

5.2 Concluding remarks

The final remarks can be summarized as following.

- The survey of the current understanding of high temperature brazing filler metal spreading phenomenon revealed a great deal of complexity and sensitivity. Although the scientific and academic contributions are steadily advancing towards understanding this complex behavior, the direct implementation of this basic knowledge in the applied field still far away from completion.
- The current practice in industry for the brazing process quality control is empirical, while the wettability test (static contact angle measurement) is used for no more than an educated guess. This wettability test is not a reliable indicator for the process success.
- The absence of the appropriate well agreed upon test to characterize the high temperature spreading of the brazing filler metal is due to the lack of a well established test concept rather than the technology to implement such a test.
- The empirical characterization of the spreading behavior of the brazing filler metal was achieved by the use an easily accessible technology.
- The spreading test results can be combined with the other experimental analysis techniques to reach a better understanding of this phenomenon.

5.3 Contributions

An approach to assess the wettability of the high temperature brazing filler metals have been proposed based on a well accepted brazing filler metal characterization method. The required test facility was designed, constructed and successfully tested to meet the

requirements of testing the wetting and spreading behavior of sensitive materials such as titanium containing Ni super alloys.

5.4 Recommendations for the future work

- The integration of the brazing filler spreading characterization technique with the currently used statistical quality control methods can result in more realistic process evaluation which in turn should relax the current specifications and enhance the process reliability.
- The long term use of the flow characterization method combined with the other metallurgical analysis can result in clear distinction of the influence of each contributing phenomena on the spreading process.
- A Significant enhancement to the apparatus can be achieved by adding a residual gas analyzer, this will enhance the ability to assess the real sample atmosphere.

References

1. M. M. Schwartz: Brazing. ASM International, Ohio, 2003, pp.1-13
2. M. D. Bellware: Fundamentals of Brazing for Elevated-temperature Service. The Welding Journal, Vol.37, No.6, 1958, pp.683-691
3. W. F. Gale: Applying TLP Bonding to the Joining Structural intermetallic Compounds. JOM, Vol.51, No.2, 1999, pp.49-52
4. D. S. Duvall, W. A. Owczarski and D. F. Paulonis: TLP Bonding a New Method for Joining Heat Resistant Alloys. The Welding Journal, Vol.53, No.4, 1974, pp.203-214
5. A. W. Adamson, A. P. Gast: Physical Chemistry of Surfaces, 6th Edition. Wiley-Interscience: New York, 1997, pp.4-43
6. J. Pellicer, J. A. Manzanares and S. Mafé: The physical description of elementary surface phenomena: Thermodynamics versus mechanics. American Journal of Physics, Vol.63, No.6, 1995, pp.542-547
7. Y. Adda, M.H. Ambroise and F. Barbier: Reactive wetting by liquid metals in materials science. Materials Science Forum, Vols.155-156, 1994, pp.511-526
8. G. Humpston and D. M. Jacobson: Principles of soldering and brazing, ASM International, 2005, pp. 268
9. D. Furrer and H. Fecht: Ni-based superalloys for turbine discs. JOM, Vol.51, No.1, 1999, pp.14-17
10. G. L. J. Bailey and H. C. Watkins: The flow of liquid metals on solid metal surfaces and its relation to soldering, brazing, and hot-dip coating. Journal of the Institute of Metals, Vol.51, 1952, pp.57-76

11. D. R. Milner: A Survey of the Scientific Principles Related to Wetting and Spreading. *British Welding Journal*, Vol.5, 1958, pp.90-105
12. J. W. Gibbs: The scientific papers of JW Gibbs Vol. I, Thermodynamics. Oxbow Press, Woodbridge, CT, 1993, pp.219-319
13. C. A. Ward and M. R. Sages: Effect of gravity on contact angle: A theoretical investigation. *Journal of Chemical Physics*, Vol.109, 1998, pp.3651-3660
14. A. I. Rusanov: Classification of line tension. *Colloids and Surfaces A: Physicochemical and Engineering Aspects*, Vol.156, No.1-3, 1999, pp.315-322
15. R. E. Johnson Jr: Conflicts between Gibbsian Thermodynamics and Recent Treatments of Interfacial Energies in Solid-Liquid-Vapor. *Journal of Physical Chemistry*, Vol.63, No.10, 1959, pp.1655-1658
16. M. E. Schrader: Young-Dupre Revisited. *Langmuir*, Vol. 11, No. 9, 1995, pp.3585-3589
17. J. J. Bikerman: The physical basis of wetting. *Colloid and Polymer Science*, Vol.218, No.1, 1967, pp.52-56
18. R. N. Wenzel: Resistance of solid surfaces to wetting by water. *Industrial and Engineering Chemistry*, Vol.28, No.8, 1936, pp.988-994
19. R. Shuttleworth and G. L. J. Bailey: The spreading of a liquid over a rough solid. *Discussions of the Faraday Society*, Vol.3, 1948, pp.16-22
20. S. J. Hitchcock, N. T. Carroll, M. G. Nicholas: Some effects of substrate roughness on wettability. *Journal of Materials Science*, Vol.16, No.3, 1981, pp.714-732

21. A. B. D. Cassie and S. Baxter: Wettability of porous surfaces. Transactions of the Faraday Society, Vol.40, 1944, pp.546-551
22. A. B. D. Cassie: Contact angles. Discussions of the Faraday Society, Vol.3, 1948, pp.11-16
23. D. Li and A. W. Neumann: Surface heterogeneity and contact angle hysteresis. Colloid and Polymer Science, Vol.270, No.5, 1992, pp.984-504
24. W. D. Harkins, A. Feldman: Films. The spreading of liquids and the spreading coefficient. Journal of the American Chemical Society, Vol.44, No.12, 1922, pp.2665-2685
25. J. F. Padday: Sessile Drop Profiles: Corrected Methods for Surface Tension and Spreading Coefficients. Proceedings of the Royal Society of London. Series A, Mathematical and Physical Sciences, Vol.330, No.1583, 1972, pp.561-572
26. F. G. Yost: Fundamentals of wetting and spreading with emphasis on soldering. Sandia National Labs, Albuquerque, NM (United States). 1991
27. F. P. Buff: The molecular hydrostatic analysis of Gibbs' theory of capillarity. Discussions of the Faraday Society, Vol.30, 1960, pp.52-58
28. F. C. Goodrich: The Mathematical Theory of Capillarity. I. Proceedings of the Royal Society of London. Series A, Mathematical and Physical Sciences, Vol.260, No.1303, 1961, pp.481-489
29. F. C. Goodrich: The Mathematical Theory of Capillarity. II. Proceedings of the Royal Society of London. Series A, Mathematical and Physical Sciences, Vol.260, No.1303, 1961, pp.490-502

30. T. D. Blake and J. De Coninck: The influence of solid–liquid interactions on dynamic wetting. *Advances in Colloid and Interface Science*, Vol.96, No.1-3, 2002, pp.21-36
31. E. J. Shaughnessy, I. M. Katz and J. P. Schaffer: *Introduction to Fluid Mechanics*. Oxford university press, New York, 2005
32. D. R. Milner and R. L. Apps: *Introduction to welding and brazing*. Pergamon Press, Oxford, 1968
33. G. Kumar and K. N. Prabhu: Review of non-reactive and reactive wetting of liquids on surfaces. *Advances in Colloid and Interface Science*, Vol.133, No.2, 2007, pp.61-89
34. H. Schonhorn, H. L. Frisch and T. K. Kwei: Kinetics of Wetting of Surfaces by Polymer Melts. *Journal of Applied Physics*, Vol.37, No.13, 1966, pp.4967-4973
35. S. Newman: Kinetics of wetting of surfaces by polymers: Capillary flow. *Journal of Colloid and Interface Science*, Vol.26, 1968, pp.209-213
36. T. P. Yin: Kinetics of spreading. *Journal of Physical Chemistry*, Vol.73, No.7, 1969, pp.2413-2417
37. R. L. Hoffman: A Study of the advancing interface 1. Interface shape in liquid-gas systems. *Journal of Colloid and Interface Science*, Vol.50, No.2, 1975, pp.228-241
38. O. V. Voinov: Hydrodynamics of wetting. *fluid dynamics*, Vol.11, No.5, 1976, pp.714-721
39. L. H. Tanner: The spreading of silicone oil drops on horizontal surfaces. *Journal of Physics D: Applied Physics*, Vol.12, No.9, 1979, pp.1473-1484

40. M. D. Lelah, A. Marmur: Spreading kinetics of drops on glass. *Journal of Colloid and Interface Science*, Vol.82, No.2, 1981, pp.518-525
41. P. G. de Gennes: Wetting: statics and dynamics. *Reviews of Modern Physics*, Vol.57, No.3, 1985, pp.827-525
42. E. B. Dussan V.: The moving contact line: the slip boundary condition. *Journal of Fluid Mechanics*, Vol.44, No.4, 1976, pp.665-684
43. E. B. Dussan: On the spreading of liquids on solid surfaces: static and dynamic contact lines. *Annual Review of Fluid Mechanics*, Vol.11, 1979, pp.371-400
44. R. G. Cox: The dynamics of the spreading of liquids on a solid surface. Part 1. Viscous flow. *Journal of Fluid Mechanics*, Vol.163, 1986, pp.169-194
45. T.D. Blake: The contact angle and two-phase flow, Ph.D. thesis, University of Bristol (United Kingdom), 1968.
46. T.D. Blake: Dynamic contact angles and wetting kinetics. *Surfactant Science Series*, Vol. 49, 1993, pp.251-309
47. S. Glasstone, K. J. Laidler and H. Eyring: *The Theory of Rate Processes*. McGraw-Hill, New York, 1941, pp.611
48. J. I. Frenkel: *Kinetic Theory of Liquids*. Oxford Univ, Press, Oxford, 1946
49. P. Petrov, I. Petrov: A combined molecular-hydrodynamic approach to wetting kinetics. *Langmuir*, Vol.8, No.7, 1992, pp.1762–1767
50. F. Brochard-Wyart and P. G. de Gennes: Dynamics of partial wetting. *Advances in Colloid and Interface Science*, Vol.39, 1992, pp.1-11
51. M.J. de Ruijter, J. De Coninck and G. Oshanin: Droplet Spreading: Partial Wetting Regime Revisited. *Langmuir*, Vol.15, No.6, 1999, pp.2209–2216

52. T.D. Blake: The physics of moving wetting lines. *Journal of Colloid and Interface Science*, Vol.229, No.1, 2006, pp.1-13
53. N. Eustathopoulos, M. G. Nicholas and B. Drevet: *Wettability at High Temperatures*. Elsevier Science, 1999, ISBN: 9780080421469, pp.419
54. E. Saiz, A. P. Tomsia, N. Rauch, C. Scheu, M. Ruehle, M. Benhassine, D. Seveno, J. de Coninck and S. Lopez-Esteban: Nonreactive spreading at high temperature: molten metals and oxides on molybdenum. *Physical Review*, Vol.76, No.4, 2007, pp.041602-041617
55. R. L. Peaslee P. F. Walter: How oxygen affects nickel brazing filler metals. *Welding Journal*, Vol.74, No.1, 1995, pp.61-67
56. K. C. Mills, E. D. Hondros and Z. Li: Interfacial phenomena in high temperature processes. *Journal of Materials Science*, Vol.40, No.9, 2005, pp.2403-2409
57. G. R. Belton: Langmuir adsorption, the Gibbs adsorption isotherm, and interracial kinetics in liquid metal systems. *Metallurgical and Materials Transactions B*, Vol.7, No.1, 1976, pp.35-24
58. E. Ricci and A. Passerone: Review: Surface tension and its relations with adsorption, vapourization and surface reactivity of liquid metals. *Materials Science and Engineering: A*, Vol.161, No.1, 1993, pp.31-40
59. E. Ricci, A. Passerone, J. C. Joudb: Thermodynamic study of adsorption in liquid metal-oxygen systems. *Surface Science*, Vol.206, No.3, 1988, pp.533-553
60. R. H. Fowler and E. A. Guggenheim: *Statistical thermodynamics*. Cambridge University Press, London, 1949, pp.422

61. S. U. Yuchu, K. C. Mills and A. Dinsdale: A model to calculate surface tension of commercial alloys. *Journal of Materials Science*, Vol.40, No.9-10, 2005, pp.1573-4803
62. J. Lee, K. Yamamoto and K. Morita: Surface tension of liquid Fe-Cr-O alloys at 1823 K. *Metallurgical and Materials Transactions B*, Vol.36, No.2, 2005, pp.241-246
63. E. T. Turkdogan, P. Grieveson and L. S. Darken: Enhancement of diffusion-limited rates of vaporization of metals. *Journal of Physical Chemistry*, Vol.67, No.8, 1963, pp.1647–1654
64. P. Costa, A. Passerone and E. Ricci: Oxygen fluxes and the measurement of the surface tension of liquid metals. *High Temperatures - High Pressures*, Vol.20, No.11, 1988, pp.59-72
65. G. Astarita: *Mass Transfer with Chemical Reaction*. Elsevier Publishing, Amsterdam, 1967, pp.188
66. E. Ricci, A. Passerone and P. Castello: Surface reactivity of liquid metal with oxygen and its relationship with surface tension measurements: a kinetic-fluodynamic model. *Journal of Materials Science*, Vol. 29, No.7, 1994, pp.1833-1846
67. P. Castello, E. Ricci, A. Passerone and P. Costa: Oxygen mass transfer at liquid-metal-vapour interfaces under a low total pressure. *Journal of Materials Science*. Vol.29, No.23, 1994, pp.6104-6114
68. A. Sakamoto: Wetting in vacuum-inert gas partial pressure atmosphere brazing. *Welding Journal, Research Supplement*, Vol.63, No.10, 1983, pp.272s-281s

69. M. McLean and E. D. Hondros: Interfacial energies and chemical compound formation. *Journal of Materials Science*, Vol.8, No.3, 1973, pp.349-351
70. A. J. Wall and D. R. Milner: Wetting and spreading phenomena in a vacuum. *Journal of the Institute of Metals*, Vol.90, 1962, pp.394-402
71. A. S. Skapski: The Surface Tension of Liquid Metals. *Journal of Chemical Physics*, Vol.16, No.4, 1948, pp.389-393
72. R. J. Klein-Wassink: Wetting of solid-metal surfaces by molten metals. *Journal of the Institute of Metals*, Vol.95, 1967, pp.38-43
73. J. G. Li, L. Coudurier and N. Eustathopoulos: Work of adhesion and contact-angle isotherm of binary alloys on ionocovalent oxides. *Journal of Materials Science*, Vol.24, No.3, 1989, pp.1109-1116
74. P. Kritsalis, J. G. Li and N. Eustathopoulos: Role of Clusters on the Wettability and Work of Adhesion of the Cu-Cr/Al₂O₃ System. *Journal of Materials Science Letters*, Vol.9, 1990, pp.1332-1335
75. I. A. Aksay, C. E. Hoge and J. A. Pask: Wetting under chemical equilibrium and nonequilibrium conditions. *Journal of Physical Chemistry*, Vol.78, No.12, 1974, pp.1178-1183
76. L. Espie, B. Drevet, N. Eustathopoulos: Experimental study of the influence of interfacial energies and reactivity on wetting in metal/oxide systems. *Metallurgical and Materials Transactions B*, Vol.25, 1994, PP.599-605.
77. K. Landry, C. Rado and N. Eustathopoulos: Influence of interfacial reaction rates on the wetting driving force in metal/ceramic systems. *Metallurgical and Materials Transactions A*, Vol.27, No.10, 1996, pp.3181-3186

78. J. C. Ambrose, M. G. Nicholas, N. Young and S. L. Jenkins: Wetting and spreading of Ni-P brazes: Effects of workpiece and braze composition. *Materials Science and Technology*, Vol.6, No.10, 1990, pp.1021-1031
79. J. C. Ambrose, M. G. Nicholas and A. M. Stoneham: Dynamics of braze spreading. *Acta Metallurgica et Materialia*, Vol.40, No.10, 1992, pp.2483-2488
80. J. C. Ambrose: Wetting and spreading of nickel brazes on steel substrates, Ph.D. thesis, University of London (United Kingdom), 1992
81. N. Sobczak, M. Singh and R. Asthana: High-temperature wettability measurements in metal/ceramic systems – Some methodological issues. *Current Opinion in Solid State and Materials Science*, Vol.9, No.4-5, 2005, pp.241-253
82. K. Schlimbach, E. F. Lugscheider, W. Tillmann, W.F. Gale: Optical Hot Stage Microscopy for Brazing Investigations. *Proceedings from Materials Solutions Conference (99)*, 1999, pp.58-63
83. E. Lugscheider, K. Schlimbach, W. Tillmann, Schaan and W.F. Gale, Auburn: Optical hot stage microscopy for brazing investigations. *DVS BERICHTE*, Vol.184, 1997, pp.180-182
84. J. M. Cohen and J. E. Castle: Analytical heating stage development for vacuum studies of brazing alloys at high temperature. *Brazing & Soldering*, Vol.5, 1983, pp.4-6
85. J. M. Cohen, J. E. Castle and M. B. Waldron: High-temperature observations of braze alloy spreading by oxide penetration. *Metal Science*, Vol.15, No.10, 1981, pp.455-462

86. K. A. Thorsen, H. Fordsmand and P. L. Praestgaard: Optical hot stage microscopy for brazing investigations. *Welding Research Supplement*, Vol.63, No.11, 1984, pp.339s-344s
87. W. D. Kingery and M. Humenik, Jr.: Surface tension at elevated temperatures. I. Furnace and method for use of the sessile drop method; surface tension of silicon, iron and nickel. *The Journal of Physical Chemistry*, Vol.57, No.3, 1953, pp.359-363
88. B. Schwarz, C. Eisenmenger-Sittner and H. Steiner: Construction of a high-temperature sessile drop device. *Vaccum*, Vol.82, No.2, 2008, pp.186-188
89. Z. F. Yuan, K. Mukai, K. Takagi, M. Ohtaka, W. L. Huang and Q. S. Liu: Surface tension and its temperature coefficient of molten tin determined with sessile drop method at different oxygen partial pressures. *Journal of Colloid and Interface Science*, Vol.254, No.2, 2002, pp.338-345
90. V. Laurent, D. Chatain and N. Eustathopoulos: Wettability of Sic by aluminium and Al-Si Alloys. *Journal of Materials Science*, Vol. 22, No.1, 1987, pp.244-250
91. X. Huang, S. Togawa, S. Chung, K. Terashima and S. Kimura: Surface tension of a Si melt: Influence of oxygen partial pressure. *Journal of Crystal Growth*, Vol.156, No.1, 1995, pp.52-58
92. Z. Jun and K. Mukal: The surface tension of liquid iron containing nitrogen and oxygen. *ISIJ International*, Vol.38, No.10, 1998, pp.1039-1044
93. J. Lee and K. Morita: Evaluation of surface tension and adsorption for liquid Fe-S alloys. *ISIJ International*, Vol.42, No.6, 2002, pp.588-594

94. W. J. O'Brien and G. Ryge: Relation between molecular force calculations and observed strengths of enamel-metal interfaces. *Journal of the American Ceramic Society*, Vol.42, No.6, 2002, pp.588-594
95. R. Lu, G. P. Görlner, H. J. Fecht and R. Willnecker: Investigation of specific heat and thermal expansion in the glass-transition regime of Pd-based metallic glasses. *Journal of Non-Crystalline Solids*, Vol.274, No.1-3, 2000, pp.294-300
96. J. Ho Lee and D. N. Lee: Use of thermodynamic data to calculate surface tension and viscosity of Sn-based soldering alloy systems. *Journal of Electronic Materials*, Vol.30, No.9, 2001, pp.1112-1119
97. M. Diemer, A. Neubrand, K. P. Trumble and J. Rodel: Influence of oxygen partial pressure and oxygen content on the wettability in the copper–oxygen–alumina system. *Journal of the American Ceramic Society*, Vol.82, No.10, 2004, pp.2825 - 2832
98. E. Ricci, E. Arato, A. Passerone and P. Costa: Oxygen tensioactivity on liquid-metal drops. *Advances in Colloid and Interface Science*, Vol.117, No.1-3, 2005, pp.15-32
99. N. Eustathopoulos, N. Sobczak, A. Passerone and K. Nogi: Measurement of contact angle and work of adhesion at high temperature. *Journal of Materials Science*, Vol.40, No.9, 2005, pp.2271-2280
100. H. D. Solomon, R. E. Delair and J. Thyssen: The High-temperature wetting balance and the influence of grit blasting on brazing of IN718. *The Welding Journal*, Vol.82, No.10, 2003, pp.278s-287s

101. N. Sobczak, R. Nowak, W. Radziwill, J. Budzioch, A. Glenz: Experimental complex for investigations of high temperature capillarity phenomena. *Materials Science and Engineering A*, Vol.495, No.1-2, 2008, pp.43-49.
102. A.C. Hall, F. M. Hosking and M. Reece: Visual observations of liquid filler metal flow within braze gap. *Science and Technology of Welding and Joining*, Vol.9, No.2, 2004, pp.95-102
103. A. Sharan and A. W. Cramb: Surface tension and wettability studies of liquid Fe-Ni-O alloys. *Metallurgical and Materials Transactions B*, Vol.28, No.3, 1997, pp.465-472
104. J. C. Ambrose and M.G. Nicholas: Wetting and spreading of nickel-phosphorus brazes: detailed real time observations of spreading on iron-chromium substrates. *Materials science and technology*, Vol.12, No.1, 1996, pp.72-80
105. Y. V. Naidich and N. F. Grigorenko: Capillary characteristics of high temperature melts measured by sessile-drop method using computer-aided TV system. *Journal of Materials Science*, Vol.27, No.11, 1992, pp.3092-3097
106. D. Sankowski and K. Strzecha: The development of image processing and analysis unit for building a solderability tester. *Instrumentation and Measurement Technology Conference, 2003. IMTC '03. Proceedings of the 20th IEEE*, Vol.1, 1992, PP.14-19.
107. P. Danielson: Anatomy of a PumpDown, *R&D Magazine*, June 2004, p. 33.
108. W. F. Gale, E. R. Wallach: Wettability of nickel alloys by Ni-Si-B fillers: influence of substrate oxide reduction and isothermal solidification. *Journal of Materials Science*, Vol. 27, No. 20, 1992, p. 5653-5660

109. C. B. Carter, M. G. Norton: Ceramic Materials Science and Engineering. Springer, 2007, PP. 147
110. J. F. Shackelford, R. H. Doremus: Ceramic and Glass Materials Structure, Properties and Processing, Springer, 2008, PP. 13
111. K. Pelissier, T. Chartier, J. M. Laurent: Silicon carbide heating elements, Ceramics International, Vol. 24, No. 5, 1998, P. 371-377
112. E. N. Kaufmann et al. : Characterization of Materials, Wiley-VCH, 2003, pp 1392
113. H. R. Brooker and E. V. Beatson: Industrial brazing, Newnes-Butterworths, London, 1975, pp 263
114. K. H.-L. Chau, et. al.: Pressure and Sound Measurement, CRC Press LLC, 2000
115. <http://vipbase.net/>
116. <http://www.markus-bader.de/MB-Ruler/>
117. <http://www.sgrillo.net/scale.htm>

Appendix A: Steps for the apparatus operation

1. Prepare the sample according to the nature and the requirements of the specific sample
2. Load the sample into the furnace chamber
3. Adjust the sample and the camera to bring the sample into focus
 - a. Start the camera and the illumination light (see the camera supporting documents)
 - b. Start the computer and the camera software
 - c. Change the camera speed to 25 fps
 - d. Adjust the camera height and the sample angle and distance until focus is achieved
4. Bake out and degas the sample and the furnace (Figure 1,2,3)
 - a. Start the argon flow
 - b. Turn-on the air
 - c. Switch the control panel power on
 - d. Switch on the mechanical vacuum pump
 - e. Adjust the argon flow until the chamber partial pressure reaches 1 torr
 - f. Turn the cooling water on
 - g. Heat to 125 °C for two hours
 - h. Stop the heating
 - i. Verify and adjust the diffusion pump cooling water flow based on the rotameter reading as marked on the device
 - j. Start the diffusion pump heater

- k. Turn the argon flow off before the diffusion pump gate opens (approximately 9 minutes after starting the diffusion pump)
 - l. Keep the diffusion pump for several hours (according to the specific sample and experiment requirements) and then turn it off
5. Test and imaging
- a. Start and adjust the argon flow till you reach the desirable pressure in the chamber
 - b. Start heating towards the test temperature
 - c. At around 900°C change to the desired frame rate and turn off the illumination if required
 - d. Further adjust the image if required and keep monitoring the sample
 - e. At the right moment trigger the camera
 - f. Turn-off the heating
 - g. When the furnace temperature reach less than 150 shut the cooling water off

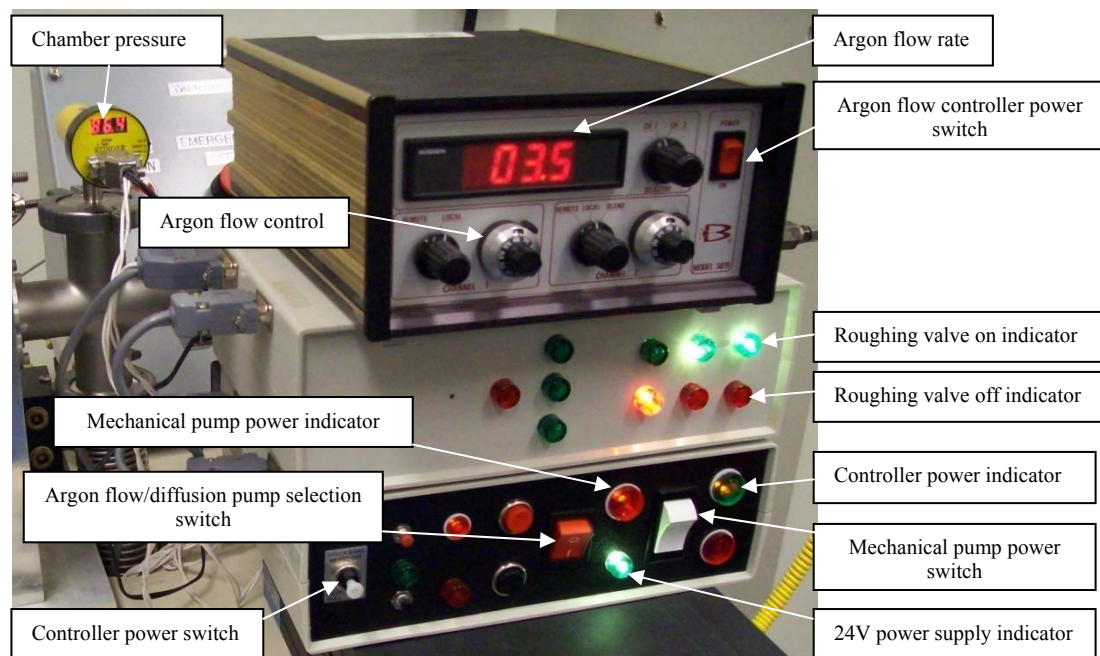


Figure 45 View of the control panel during roughing vacuum



Figure 46 View of the heating controller

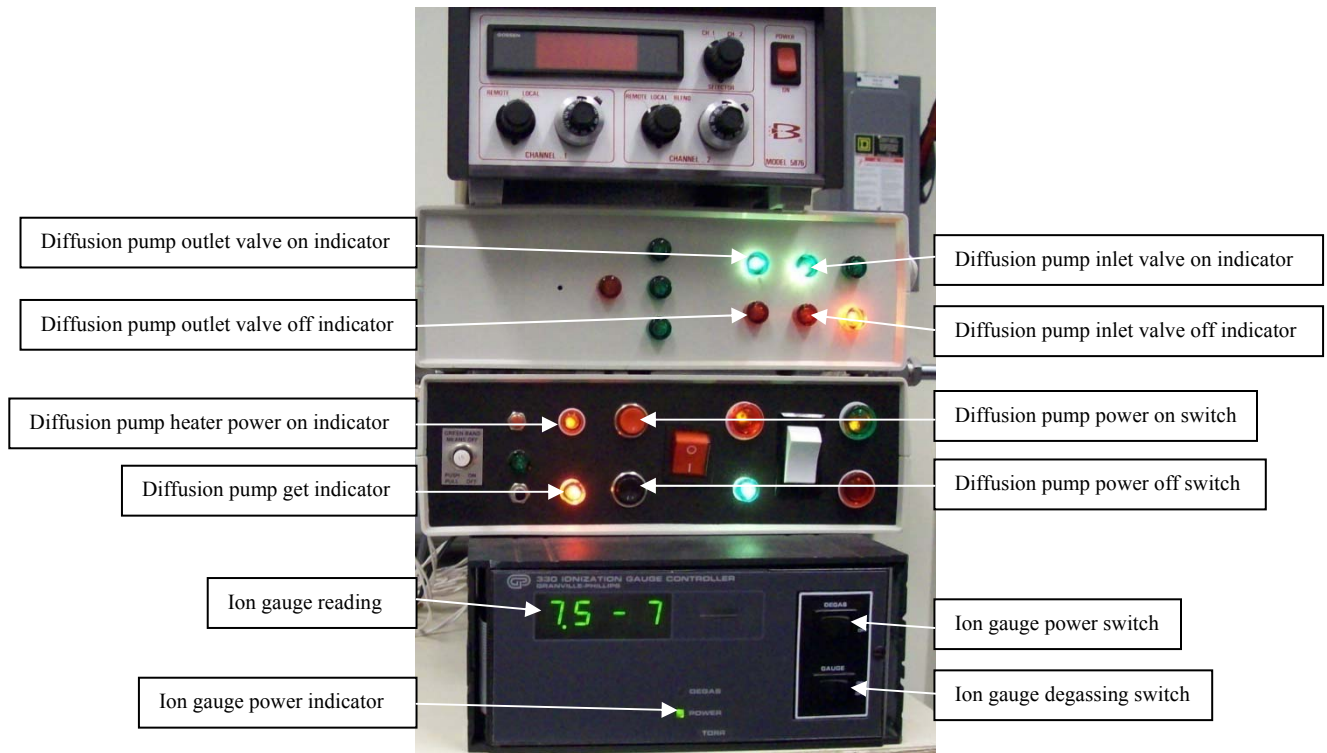


Figure 47 View of the control panel during diffusion pump operation



Figure 48 View of the control panel during argon flow operation